DESIGN AND FABRICATION OF AN OSMOTIC PRESSURE SENSOR FOR GLUCOSE SENSING APPLICATION

NAGESH CH

DESIGN AND FABRICATION OF AN OSMOTIC PRESSURE SENSOR FOR GLUCOSE SENSING APPLICATION

A

Thesis Submitted

in Partial Fulfillment of the Requirements

for the Degree of

DOCTOR OF PHILOSOPHY

by

NAGESH CH

DEPARTMENT OF ELECTRONICS AND ELECTRICAL ENGINEERING

INDIAN INSTITUTE OF TECHNOLOGY GUWAHATI

GUWAHATI-781039, ASSAM, INDIA

May, 2015

To

My dear parents

Manaiah Ch and Yadamma Ch

My Dear In-Laws

K Narsaiah and Pichhamma

for their love and support

My guide

Prof. Roy P Paily

for his guidance and inspiration

DECLARATION

*This is to certify that the thesis entitled "**DESIGN AND FABRICATION OF AN OSMOTIC PRESSURE SENSOR FOR GLUCOSE SENSING APPLICATION**", submitted by me to the Indian Institute of Technology Guwahati for the award of the degree of **Doctor of Philosophy** is a bonafide work carried out by me under the supervision of **Prof. Roy P Paily** . The contents of this thesis, in full or in parts, have not been submitted to any other Institute or University for the award of any degree or diploma.*

Signed:

NAGESH CH

Department of Electronics & Electrical Engineering,

Indian Institute of Technology Guwahati,

Guwahati-781039, Assam, India.

Date:

CERTIFICATE

*This is to certify that the this thesis entitled "**DESIGN AND FABRICATION OF AN OSMOTIC PRESSURE SENSOR FOR GLUCOSE SENSING APPLICATION**" submitted by **NAGESH CH (08610208)**, a research scholar in the Department of Electronics and Electrical Engineering, Indian Institute of Technology Guwahati, for the award of degree of **Doctor of Philosophy**, is a record of an original research work carried out by him under my supervision and guidance. The thesis has fulfilled all requirements as per the regulations of the institute and in my opinion has reached the standard needed for submission. The results embodied in this thesis have not been submitted to any other University or Institute for the award of any degree or diploma.*

Signed:

Supervisor: Prof. Roy P Paily
Department of Electronics & Electrical Engineering,
Indian Institute of Technology Guwahati,
Guwahati-781039, Assam, India.

Date:

Acknowledgments

First and foremost, I feel it as a great privilege in expressing my deepest and most sincere gratitude to my supervisor Prof. Roy P Paily, for his excellent guidance throughout my study. My heartfelt thanks to you Sir, for the unlimited support and patience shown to me. He has also created an indispensable environment for me to conduct my project work. I would particularly like to thank him for all his help in patiently and carefully correcting all my manuscripts. I could not have imagined having a better advisor and mentor for my Ph.D study.

I am also very thankful to my doctoral committee members Prof. Anup Kumar Gogoi, Prof. Harshal B. Nemade and Dr. Hemangee K. Kapoor for sparing their precious time to evaluate the progress of my work. I would also like to thank the Head of the Department and the other faculty members for their kind help in carrying out this work. I am also grateful to all the members of the research and technical staff of the department without whose help I could not have completed this thesis.

I owe my deepest gratitude to Prof. K N Bhat for accepting our proposal and to use the fabrication facilities in the Center for Nano Science and Engineering (CeNSE) at IISc, Bangalore under INUP. Sir, I am fortunate to have the opportunity to work with you. The most valuable time you had spent in reviewing the proposal and discussing the process steps in detail were very useful to my work. My sincere thanks to Dr. Sanjeev Kumar Shrivastava for his help during my stay at IISc. I am thankful to Dr. Savitha, Pavani Vamsi Krishna, Srinivas Murthy, Amod Hulge, Suman Gupta, Ragupathy, Tejaswini, Vijay Monterio, Soumya Mariam Sam, Pavandeep, Radha B, Grace Mathew Abraham, Sabiha Sultana and staff members of CEN for their support during the fabrication process. A special thanks to the Prof. M M Nayak and Mr. Pandian of the CeNSE for their constant support during the packaging of the device.

I would like to extend my sincere thanks to all my beloved friends at the VLSI Laboratory. They have always been around to provide useful suggestions, companionship and created a peaceful research environment. They all contributed directly or indirectly to this thesis. My special thanks to Mrs. Josphene madam for her help in all respects. I thank Dr. Genemala,

Mr. Sanjib Das, Dr. KCN Murthy, Ashish, Naveen suda, Ramesh, Gaurav, Rahul, Pronjol, Vinaya, Saroj, Brajesh, Pavan, and for their friendly support during my stay at IITG.

I thank all my fellow research students and M. Tech students for their cooperation. During my stay at IITG I have had several friends that have helped me in several ways, I would like to say a big thank you to all for your friendship and support.

I am really thankful to God for the Guwahati church and friends. The friendship and unforgettable attachments shared with them has made my life pleasant. I extend my indebted gratitude towards the church, with whom I cherished my good times, for their support and encouragement in due times and their prayers.

My deepest gratitude goes to my family (In-Laws and sisters) for their continuous love and support throughout my studies. Words cannot express how grateful I am to my mother, father and brother for all of the sacrifices that they have made on my behalf. I extend my indebted gratitude towards my brother In-Law (S Vittal) and uncle (Buddapuli Narsimulu and G Venkat Swamy) for their support and motivation throughout my journey.

I extremely thankful to Peetala Ravi Kumar for the care shown and the help given to me during my stay at IITG. Special thanks to P Venkat (my friend) for your support and help, specially during my M Tech and Ph D. You are the one whom i can look at all the time without hesitation.

I owe my loving thanks to my wife Kanchana Katta, and my son Joel without their encouragement and understanding it would have been impossible for me to finish this work.

Finally, I believe this research experience will greatly benefit my career in the future.

NAGESH CH

Abstract

The main objective of this thesis is to provide the design and fabrication aspects of an osmotic pressure sensor for glucose sensing application.

First, we present the design and simulation of a SiO_2 microbridge which measures the differential surface stress induced by the adsorption of molecules. Materials with smaller Young's modulus would be appropriate to measure the small variation of surface stress on the microbridge and therefore SiO_2 is chosen as the material for microbridge. The SiO_2 microbridge may be used for glucose detection if the enzyme glucose oxidase is immobilized on a top surface. The mechanical behavior of the SiO_2 microbridge and the electrical response of the piezoresistors are analyzed using the FEM (Finite Element Method). The dimensions for the microbridge are optimized by considering both the sensitivity and nonlinearity with respect to the deflection. The placement location of the piezoresistors and the effect of geometrical parameters of the piezoresistors on the sensitivity SiO_2 microbridge are studied. The obtained sensitivity, $\Delta R/R$ of SiO_2 microbridge is 6.15×10^{-4} which is four times higher than that of existing work.

A chemical reaction free, pressure sensor, based on osmosis principle has been designed for sensing the concentration levels of an osmotically active substance. The device consists of a square cavity on the bottom side with a thin Si membrane on the top. The square cavity filled with a glucose solution of 100 mg/dL as a reference solution, and it is sealed with a semi-permeable membrane. The fluid flow across semi-permeable membrane, and mechanical as well as the electrical behavior of the device are analyzed using FVM (Finite Volume Method) and FEM commercially available software tools. The geometrical parameters of the device are optimized to improve the sensitivity and linearity.

The pressure sensor is fabricated using the bulk micromachining technology, on the SOI (silicon on insulator) wafer. Two sets of devices, having membrane thickness of 10 μm and 25 μm, but the same area of 3 mm $\times$ 3 mm are fabricated. A cost effective packaging method for the individual device is suggested. The device is embedded in a PCB for the wire bonding. After wire bonding, the device is assembled into a square cavity of polycarbonate (PC) material. The

piezoresistive pressure sensor is packaged using the PC by employing simple technique avoiding costly steps such as laser dicing, etching, lithography and anodic bonding. Further, all the device packaging steps are carried out at low temperature.

The performance and repeatability of the piezoresistive pressure sensor are tested initially by applying the external gas pressure. Subsequently, glucose solution is employed to prove the functionality of the device and it is tested for the different glucose concentration levels ranging from 50 mg/dL to 450 mg/dL. The output voltage obtained for the corresponding glucose concentration levels are from -6.7 mV to 22.7 mV for the 10 μm device and from -1.7 mV to 4 mV for the 25 μm device. The simulation and experimental results are closely matched. A response time 40 min is obtained in the case of 10 μm device, compared to 30 min for the 25 μm device. The response time obtained for these devices are found to be smaller compared to similar works based on osmosis principle. This pressure sensor has the potential for controlled drug delivery if it can be integrated with other microfluidic devices.

Finally, we have designed an AC electro-osmotic pump for controlled drug delivery. The micro-pump consists of four arrays of traveling wave electrodes on a glass substrate. The input AC voltage of amplitude 1 V at a frequency 500 Hz is switched between the four sets according to the requirement of insulin delivery. The set1 operates continuously and delivers background insulin with a flow velocity approximately 32 μm/s. If this micro-pump is integrated with a continuous glucose monitoring system, it can deliver insulin according to the glucose concentration levels and the combined system can serve as an artificial pancreas.

Keywords: Diabetes, Drug delivery, Electro-osmotic pump, Glucose, Fabrication, Micro-bridge, Osmosis, Packaging, Piezoresistive pressure sensor, Semi-permeable membrane.

Contents

List of Figures

List of Tables

List of Acronyms

2D	Two dimensional
3D	Three dimensional
A	Membrane area (m^2)
A_p	Overlap area between the two plates (μm)
AAO	Anodic Aluminum Oxide
AFM	Atomic Force Microscopy
ALE	Arbitrary Lagrangian-Eulerian
b	Width of the microbridge (μm)
BEM	Boundary Element Method
BHF	Buffered Hydrofluoric Acid
BN	Boron Nitride
BSG	Borosilicate Glass
C	Capacitance (F)
$C_6H_{12}O_6$	D-glucose
CA	Cellulose Acetate
Con A	Concanavalin A
D	Diffusion coefficient (m^2/s)
DRIE	Deep Reactive Ion Etching
d	Separation between electrodes (μm)
d_m	Semi-permeable membrane thickness (μm)
d_p	Particle diameter (Å)
DI	Deionized

E	Young's modulus (Pa)
E_i	Electric field (V/m)
EMC	Epoxy molding compound
FEM	Finite Element Method
FVM	Finite Volume Method
f_0	Frequency (Hz)
F	Force (μN)
FO	Forward Osmosis
GOx	Glucose oxidase
G	Shear modulus (Pa)
H	Height of the device cavity (μm)
h	Thickness (μm)
HF	Hydrogen fluoride
H_2O_2	Hydrogen peroxide
i_i	Current density (A/m^2)
I	Moment of inertia (m^4)
IC	Integrated Circuit
IPA	Isopropyl Alcohol
J_v	Flow rate (m^3/s)
K_P	Filtration coefficient (m^2)
KCl	Potassium Chloride
L	Length of the microbridge (m)
l_0	Half of side length of the membrane (mm)
l	Length of the membrane (mm)
L_m	Length of the Si membrane (mm)
L_R	Length of the piezoresistor (μm)
M_A, M_B	Bending moments at the support A and B (N·m)
MWCO	Molecular Weight Cut off

MEMS	Microelectromechanical Systems
NaCl	Sodium Chloride
O_2	Oxygen
P	Pressure (Pa)
PECVD	Plasma Enhanced Chemical Vapor Deposition
PC	Polycarbonate material
PCB	Printed Circuit Board
PPR	Positive Photoresist
Pt	Platinum
PA	Polyamide
PZR	Piezoresistor
q	Concentrated load (N/m)
R	Gas constant (8.3145 J/K·mol)
R_A, R_B	Reaction forces at the support A and B (N)
RIE	Reactive Ion Etching
RO	Revers Osmosis
Si	Silicon
SiC	Silicon carbide
Si_3N_4	Silicon nitride
SiO_2	Silicon dioxide
SOI	Silicon on Insulator
SAW	Surface Acoustic Wave
t	Response time (min)
T	Temperature (K)
Ti	Titanium
t_R	Thickness of the piezoresistor (μm)
V	Volume change (m^3)
w	Displacement (μm)

W_R	Width of the piezoresistor (μm)
$Z(l)$	Bending in a membrane (μm)
ZnO	Zinc oxide

Greek Symbols

ω	Angular frequency (rad/s)
ΔC	Concentration difference (mg/dL)
ρ	Density (kg/m^3)
$\Delta\sigma$	Differential surface stress (N/m)
η	Dynamic viscosity of a fluid (Pa·s)
λ_D	Debye length (nm)
ΔP	Hydrostatic pressure difference (Pa)
$\Delta\pi$	Osmotic pressure difference (Pa)
ϵ	Permittivity (F/m)
π_{11}, π_{12}, π_{44}	Piezoresistive coefficient's (Pa^{-1})
ν	Poison's ratio
ϕ	Porosity
$\Delta\phi$	Potential drop across the diffuse double layer (V)
σ	Reflection coefficient of membrane
σ	Conductivity (S/m)
$\frac{\Delta R}{R}$	Sensitivity of the microbridge
ρ_0	Stress free resistivity (Ω-cm)
σ_l	Stress (l refer to longitudinal stresses) (Pa)
σ_S^+, σ_S^-	Surface stress (N/m)
k	Thermal conductivity (pW/μmk)

1

Introduction

Contents

1.1 Diabetes and Glucose Sensing Devices

Diabetes mellitus is a metabolic disorder, which once diagnosed is not reversible and is characterized by imbalance in blood glucose levels. This imbalance is due to the lack of insulin production from the pancreas or inability of the body to use endogenous insulin effectively, and therefore a regular monitoring of blood glucose levels is inevitable to manage the insulin intake. This is to avoid further complications like heart disease, nerve damage, kidney failure, and vision disorders etc. The continuous monitoring of abnormal glucose levels in a diabetes patient is carried out by either non-invasive or minimally invasive approaches. Non-invasive method of glucose detection is observed using optical devices, by directing a light beam through the skin, to measure the properties of the reflected light. Generally, such method has limited accuracy and

reliability [1, 2]. Approximately, 85% of the entire biosensor market consists of electrochemical glucose biosensors [3]. One of them is fingerstick meter readings, and it would require at least 4-5 blood samples per day. This method is fast and accurate, but it is a tedious process and will be painful in the long run [4]. Minimally invasive, subcutaneously implanted electro-enzymatic glucose detection devices are most popular among all the techniques. The change in glucose concentration is proportional either to the consumption of oxygen (O_2) or to the production of hydrogen peroxide (H_2O_2) [5]. Electro-enzymatic methods of glucose detection are simpler, faster and sensitive. This technique is the basis for a number of commercially available devices such, as Glucose Analyzer[6], MiniMed Paradigm Real-Time Revel System [7], FreeStyle Insulinx Meter [8], and Dexcom G4 Platinum [9]. The drawback of the electro-enzymatic detection is the irreversible consumption of glucose, and this might change the equilibrium concentration of glucose in tissue, and as a result it affects the actual measured glucose level [10, 11]. Moreover, the rate of glucose consumption is diffusion limited, and depends on the active nature of diffusion layer. The sensitivity of the sensor affects greatly, if there is any change in the diffusion layer during the chemical process. Other drawbacks of this method are the interference from the electrode-active chemicals (such as ascorbic acid, catechol, uric acid, and acetaminophen) during the H_2O_2 production [12].

The advancement in the field of micro-machining technology has helped the fabrication of different kinds of microelectromechanical system (MEMS) devices such as bridges, microactuators, pressure sensors, micro-cantilevers and drug delivery pumps. These MEMS devices have emerged as a standard platform for biomedical applications, including ultrasensitive mass measurements, biomolecular sensing, and detection of chemical analytes, diagnostic and glucose monitoring. The enzyme glucose oxidase (GOx)-based micro-machined silicon (Si) cantilever has been fabricated and demonstrated successfully [12]. The basic principle is similar to electro-enzymatic detection, but instead of measuring the O_2 consumption or the production of H_2O_2, the deflection due to the surface stress is analyzed to quantify the glucose concentration levels [13, 14]. A major advantage of this technique is the selectivity, because of the high selectivity of GOx. Moreover, the response of the device is degraded when the experiment is repeated

multiple times, and it may be due to the corrosive effect of H_2O_2 on the enzyme layer.

The above-mentioned drawbacks of electro-enzymatic detection motivated the researchers to investigate a chemical-free glucose sensor. Osmosis is a passive transportation of a solvent (water) across the semi-permeable membrane driven by a concentration difference. The osmotic sensors employ the natural phenomenon called osmosis, which occurs in many biological systems including the human body [15]. Frederic N and Ruedes E [16], fabricated an implantable device to measure the glucose levels. The device has two pressure sensors, and the chamber of each sensor is sealed with two different membranes. The in/out fluid flow across the membranes create a volume change inside the chamber of the respective sensors. The change in osmotic pressure difference is quantified in terms of change in capacitance and the signal of interest is the difference between the two pressure sensors. However, the sensitivity and accuracy are limited because the change in capacitance which is very small compared to the fixed capacitance. Nagakura et al. [17], developed an auto-regulated osmotic pump for insulin delivery. This system consists of an osmotic pump which is attached to a microsyringe. Osmotic pump is filled with standard glucose solution (100 mg/dL) and sealed by the semipermeable membrane. When concentration outside the pump increases, the solvent is drawn out from the pump and volume of fluid in pump decreases and hence the membrane bends. The displacement in the membrane provides the needed mechanical stroke to the microsyringe which delivers the required amount of insulin. However, the system does not have any in-built sensing mechanism to monitor the glucose concentration levels. Moreover, the size of their system and its response time are very high. Ellingsen O [18], proposed a device to measure the osmotically active substance in the body fluid. It is capable of continuous glucose monitoring since the system is employed with a feedback loop. The hindrance with this design is the fact that a significant amount of water must be transported through the membrane when the osmolality in the body is changing to move the position of a piston up and down, as the result sensitivity reduced. Moreover, the system is large in size and has longer response time. Further, the use of osmotic energy is successfully demonstrated to provide the mechanical actuation in a microactuator for the drug delivery applications [19, 20]. Event hough, the operation of these devices are free of

any chemical reactions, but they suffer from sensitivity, response time, and size related issues. In another approach, smart hydrogels are confined inside a pressure sensor to facilitate the measurement of change in glucose concentration levels [21, 22, 23]. Though, its response time is high, the inclusion of smart hydrogels offers high sensitivity and selectivity.

Insulin pumps are used to deliver exogenous insulin to compensate lack of indigenous insulin from the pancreas. These pumps act as artificial pancreas for delivering insulin but it cannot sense the glucose levels automatically like the pancreas in a human body. There are different ways to take the insulin into the human body, most popular methods are intravenous, subcutaneous, and intraperitoneal routes [4]. In all these external infusion techniques, infection risks are very high. The conventional insulin delivery pumps use mechanical strokes [17] to deliver insulin and it may lead to error in the infusion because of the aging problems in the mechanical parts.

1.2 Motivation and Problem Statement

The problems associated with the above mentioned devices have motivated us to design and fabricate a sensor with better response time, improved sensitivity, chemical-free nature, avoidance of any mechanical excitations, linearity and improved life time. Further, there should be provision for the integration of electronic circuit with glucose sensing devices. This thesis aims at the design and fabrication of an osmotic pressure sensor for glucose sensing application, while improving its performance by identifying the various tradeoffs that exist among the performance parameters.

Through a simulation study, we will investigate, initially, a high sensitivity micro-bridge for the measurement of differential surface stress due to the adsorption molecules. The micro-bridge provides the necessary stability in different conditions compared to microcantilever, because of its two ends support. The micro-bridge could be developed as a potential device for the continuous monitoring of glucose levels. Moreover, it provides the selective detection of glucose, if the GOx was immobilized on a top surface of the micro-bridge.

The design, fabrication, packaging and testing of an osmotic pressure sensor to measure

the glucose concentration levels will be the main focus of the thesis. In order to optimize the design of an osmotic pressure sensor, we have first fine tuned its performance parameters using simulation studies. The FEM (Finite Element Method) is used for the electro-mechanical analysis of pressure sensor and the FVM (Finite Volume Method) is employed for the fluid flow analysis across a porous medium. The geometrical parameters of the system plays a major role and they decide the response time, sensitivity and linearity of devices. By considering these effects, two sets of devices having membrane thickness of 10 μm and 25 μm are designed and their results are compared with respect to each other. The designed osmotic pressure sensor is fabricated by employing a bulk micro-machining technology on a SOI (Silicon on Insulator) substrate. The advantage of using the Si material over the polymer material is that the electronic circuit can be integrated on the same substrate. After the fabrication, the device is packaged such that it can interact with liquids, gases or to any external pressure ambients. The device is packaged using the polycarbonate (PC) material by employing a simple technique instead of following the standard procedure such as a laser dicing, plasma cleaning, wet/dry etching, lithography and anodic bonding for the packaging. The performance of the packaged device was demonstrated successfully for the different glucose concentrations ranging from 50 - 450 mg/dL with respect to the reference solution. Further, the simulation results of the designed osmotic pressure is compared with experimental results.

Finally, an AC electro-osmotic pump is designed for the controlled drug delivery application. The electro-osmotic pump may be integrated with glucose sensor since there are no moving parts involved to deliver the required amount of insulin according to the glucose concentration levels.

1.3 Summary of Contributions and Results

A brief description major contribution is as follows (Fig. 1.1);

1.3.1 Design of a micro-bridge for Glucose Sensing Application

A micro-bridge which measures the differential surface stress induced by the adsorption of molecules has been designed. In this work, silicon dioxide (SiO_2) is chosen as the material for the

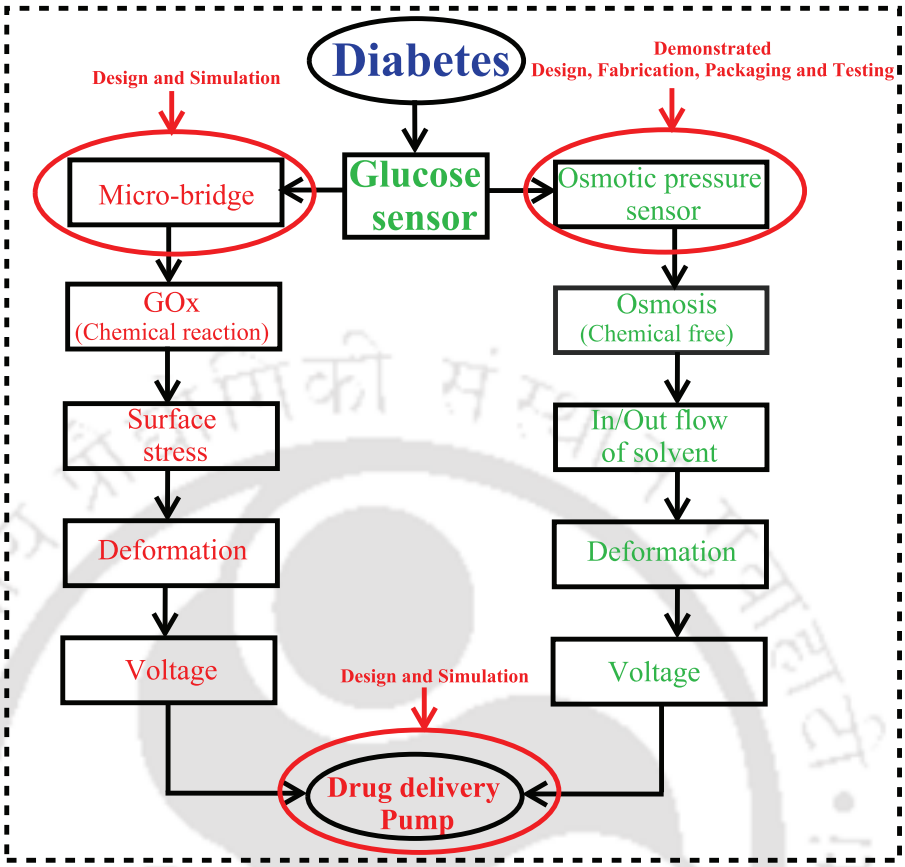

Figure 1.1: Flow chart summarizes the major contribution.

micro-bridge. The unique characteristic of a micro-bridge is that it bends when the molecular adsorption by confined to one side of the surface. The deflection in micro-bridge is measured in terms of change in the resistance of a piezoresistors which are diffused on the top layer of Si. The piezoresistors are placed at the edges of the micro-bridge, as the maximum stress is at the edges compared to the middle. To improve the sensitivity, we have used two piezoresistors instead of one along the micro-bridge [24]. Moreover, enough space is provided between piezoresistors at the top surface of the micro-bridge and it can be used for the adsorption of molecules, instead of the bottom surface. The deposition of active layer on top surface is very easy compared bottom surface. FEM is used to analyze the electrical and mechanical response of a piezoresistor based micro-bridge.

The dimensions of the micro-bridge are chosen as 400 μm $\times$ 50 μm $\times$ 1 μm by considering both the nonlinearity and sensitivity aspects with respect to the deflection. The peizoresistors

are p-type boron doped Si with the doping concentration of 1×10^{17} cm^{-3}. The maximum change of $\Delta R/R$ is 0.00568 for a width of 2.5 μm and a thickness of 0.25 μm piezoresistors. The thickness of the piezoresistors has more significant effect on the sensitivity of the micro-bridge compared to the width of the piezoresistor, though both can affect the deformation as well as the $\Delta R/R$ of micro-bridge. The placing of piezoresistors on the micro-bridge and the optimization of the geometrical parameters of the piezoresistors are the reasons for the improved performance. The small variation in the resistance of piezoresistors as the result of differential surface stress on the micro-bridge is observed in terms of output voltage. The change in output voltage of the SiO_2 micro-bridge is from 0 to 1.472 mV, when the force value is varied from 0 to 2 μN. The output voltage obtained is twice since the change in resistance of two piezoresistors are considered instead of single piezoresistor. Thus, the micro-bridge has the potential for the glucose sensing with high sensitivity and selectivity, if GOx could be immobilized on its surface.

1.3.2 Design of an Osmotic Pressure Sensor

The osmotic pressure sensor consists of an actuation membrane on the top side and it is constructed on a SOI substrate by making a square cavity on the bottom side using bulk micro-machining technique. The square cavity used to fill the glucose concentration of 100 mg/dL as a reference solution and it sealed with a semi-permeable membrane. When the device is exposed to the fluid outside, having the same solution but with a different concentration, an osmotic pressure difference across the semi-permeable membrane is created and it leads to the flow of solvent in/out.

The osmotic pressure sensor measures the change in glucose concentration levels. For example, when the glucose concentration outside the device is 150 mg/dL, the concentration difference is 50 mg/dL. Due to such a concentration difference, the solvent flows across the semi-permeable membrane to the higher concentration side. Equation (1.1) describes the rate of solvent flow through the semi-permeable membrane [25].

$$J_v = \frac{K_p}{\eta d_m} A(\sigma \Delta\pi - \Delta P) \tag{1.1}$$

where K_p is the filtration coefficient, J_v is the volume flow of solvent per unit time, A is the surface area of the membrane, σ is reflection coefficient of membrane, η is the dynamic viscosity of the fluid, d_m is the membrane thickness, $\Delta\pi$ and ΔP are the differences in osmotic and hydrostatic pressure respectively. The in/out flow of solvent through a semi-permeable membrane creates a volume change inside the cavity and leads to the deformation of a Si membrane on the top side. The deformation in the Si membrane is high because of the fact that semi-permeable membrane is stiff and it is thicker. The deformation in Si membrane is measured in terms of change in resistance. The sensors contain sensing elements (piezoresistors) made up of a P-type Si because its sensitivity is more compared to an N-type silicon. Finally, the output voltage of the Wheatstone bridge circuit, by considering geometry of piezoresistor and doping concentration, is given by equation (1.2).

$$\frac{V_o}{V_s} = (\pi_{44} \times 0.141)(\frac{l}{h})^2(\frac{W_R}{L_R})\Delta P \tag{1.2}$$

where l is the length of the membrane, h is the thickness of the membrane, π_{44} is the piezoresistive coefficient, W_R and L_R are width and length of the piezoresistor respectively. Compared to capacitive or piezoelectric types, piezoresistive pressure transducers are easer to fabricate and provide a linear variation in resistance with respect to the stress being measured.

Initially, fluid flow through the semi-permeable membrane is studied. Then, the relation between fluid and structure interactions are analyzed by coupling three different equations. The Navier-Stokes equation solves the fluid flow through the porous medium, and Arbitrary Lagrangian-Eulerian (ALE) method handles the dynamics of structural deformation. The change in glucose concentration levels outside the device are measured with respect to the reference solution. When the device is exposed to the glucose solution of different concentration, for example 150 mg/dL, the flow of solvent starts from the device through the semi-permeable membrane as long as the $\Delta\pi$ is higher than ΔP. The output voltage across the Wheatstone bridge is increased from 0 to 21.2 mV approximately after 40 min for a device having Si membrane dimensions 3 mm $\times$ 3 mm $\times$ 10 μm. The sensitivity is 2.10 - 1.45 mV/V/kPa when the membrane dimensions are 3.5 mm $\times$ 3.5 mm $\times$ 10 μm which is high compared to a devices

having two different thickness of 10 μm and 25 μm but the same area of 3 mm $\times$ 3 mm. The nonlinearity will be more if the membrane thickness is small. The nonlinearity is 12.65 % approximately for the case of device having dimensions 3.5 mm $\times$ 3.5 mm $\times$ 10 μm which is very high compared to 3.29 % and 0.82 % for the devices having two different thickness of 10 μm and 25 μm but the same area of 3 mm $\times$ 3 mm. The thickness of the Si membrane defines the amount of solvent that moves in/out of the device. The response time can be decreased by constraining the deformation of the Si membrane, that is, by increasing the thickness of the membrane. By considering the response time, linearity and sensitivity, finally, we have decided to fabricate two devices having different diaphragm thickness of 10 μm and 25 μm, but having the same area of 3 mm $\times$ 3 mm.

1.3.3 Fabrication and Packaging of an Osmotic Pressure Sensor

The designed piezoresistive pressure sensor is fabricated using bulk micro-machining technology. The SOI substrate of an N-type material as device layer is used for the sensor fabrication. Initially, SiO_2 is deposited on the substrate using a wet oxidation technique. The next step is the boron diffusion on to the front side of the substrate for the piezoresistors. After the boron diffusion process, the SiO_2 is deposited on the bottom side of substrate using plasma enhanced chemical vapor deposition (PECVD) technique and it will be used as mask during Si etching. The square cavity is constructed on the SOI substrate by etching the bulk Si from the bottom side using DRIE. The final step is metallization, and a thermal evaporation technique is employed, to provide the metal contacts for the piezoresistors. After the device fabrication, the metal contacts and resistance values of the piezoresistors are checked using DC probe-station (Agilent 4155C), by applying current as the input and the output is voltage drop across the resistors.

The packaging involves several processing steps, beginning with the dicing of device and concludes with the sealing of device for the mechanical protection, each stage is monitored to meet the desired performance. The wafer is diced using the diamond cutter to separate the individual devices. A printed circuit board (PCB) is designed and fabricated, with metal bond

pads made of gold and a square shaped window is provided in the center for the device housing. The device is bonded into the PCB using a die bonding epoxy adhesive and it is cured at a temperature of 150° C for 60 min. The electrical contact between the metal bond pad of the device and the pad on the PCB is made by wire bonding. After the wire bonding, the device packaging is initiated. Polycarbonate (PC) material is chosen as the packaging material. The PC flat sheet is diced into the rectangular plates according to the desired dimensions. The square window is opened in the middle of the rectangular plate using a Lathe machine. This is to provide the housing for the PCB, which contains the device. The PCB is mounted in a PC flat sheet, and the device cavity on the bottom side is kept open such that it can interact with the environment (osmotic liquids, gases, and external pressure). Finally, the top side is sealed with the square cavity cap made up PC flat sheet to provide mechanical protection as well as isolation for electrical contacts from fluids. Depending on the application, the top side square cavity cap can be sealed permanently, or else a locking system is provided between the top and the bottom plate.

After packaging, the performance of the device is tested by applying an external pressure. During the packaging, a provision was provided to facilitate the application of external pressure on the bottom side of the device. The pressure applied is from 0 to 30 mmHg and the corresponding voltage across the Wheatstone bridge configuration is 0 to 18 mV. The sensitivity of the pressure sensor is 0.120 mV/mmHg/V. The above data confirms that the device is suitable for low pressure sensing applications.

1.3.4 Experimental Setup and Testing of an Osmotic Pressure Sensor

A test setup is prepared for the glucose sensor to measure any change in glucose concentration levels. To begin the testing, the square cavity is filled with a glucose solution of 100 mg/dL and sealed with a semi-permeable membrane. To characterize the device response time, the glucose concentration in the square cavity need to be reset to the reference value of 100 mg/dL i.e. the output voltage need to brought back to the reference value (close to zero). For

this purpose, prior to the test of a new concentration, every time, a glucose solution of 100 mg/dL is introduced into the test chamber, where it is allowed to permeate through the semi-permeable membrane. Next, the test chamber which contains a glucose solution of 100 mg/dL is replaced with another liquid under test (in this case a 150 mg/dL solution). The concentration difference is 50 mg/dL across the semi-permeable membrane and the corresponding osmotic pressure developed as per equation (1.1). The resultant change in output voltage, corresponds to 150 mg/dL glucose concentration, is continuously monitored. The voltage, finally, reaches a maximum value of 21.6 mV after 40 min and for further 10 min, the variation observed is negligible. The sensitivity (output voltage per [mg/dL] per voltage per time) for the 25 μm device is approximately 0.5 μV/(V·mg/dL·min) and it is low compared to 10 μm device which is 2 μV/(V·mg/dL·min), without any amplification of the output voltage. The disadvantage of increasing membrane thickness is that the sensitivity will be reduced.

The glucose sensor is tested with different glucose concentrations ranging from 50 mg/dL to 450 mg/dL. The time needed to reach the maximum value of the output voltage is different for each concentration and it is shortest for a case where the test chamber contains the highest concentration of glucose. For instance, when the glucose solution in the test chamber is 450 mg/dL, the output voltage attains its steady state value within 15 min. When the concentration is increased from 50 mg/dL to 450 mg/dL, the output voltage across the Wheatstone bridge is increased from -6.7 mV to 22.7 mV for the 10 μm device. The output voltage indicated in each case is the value obtained after 15 min of osmosis. The simulation results and the experimentally obtained values are in close agreement for the 25 μm device. However, a slight deviation is observed between simulation and experimental results for the 10 μm device and the error is about 10 %. The sensitivity can be increased by employing a smaller membrane thickness, at the cost of increasing response time and nonlinearity. The device life time of the present sensor is expected to be longer since there are no chemical reactions are involved. The response time obtained for the devices having two different thickness 10 μm and 25 μm are 40 min and 30 min respectively, and it is smaller compared to similar works based on osmosis principle.

1.3.5 Design of a Controlled Drug Delivery Pump

The AC electro-osmotic micro-pumps seem to be promising for the drug delivery at micro and nano-scale, due to the absence of moving parts and it is relatively easy to integrate with a glucose sensor. In this section, we present the design of an AC electro-osmotic pump for the insulin delivery application. The flow velocity is increased by increasing the number of electrodes which are placed on both sides of the channel wall. The electrodes in the micro-pump are driven by low amplitude AC voltage of low frequency f_0 and therefore suitable for low power portable devices. The low frequency is chosen to avoid any transient effects and to maintain the unidirectional fluid flow. An additional advantage of employing low-voltage is the absence of electrolysis in the system.

The micro-pump consists of an array of 48 interdigitated electrodes coated on a glass substrate. The electrodes are 20 μm wide and separated by distance of 20 μm. These electrodes are arranged into four sets. The advantage of this method is that the micro-pump delivers the insulin with different flow rates according to the glucose concentration levels. The set1 operates continuously to provide the background minimum insulin needed for the patient. If the glucose concentration levels are increased after the food intake, the input voltage is switched from set1 to set2, or to set3 or to set4, depending on the insulin requirements. If more insulin is to be delivered, more than one set can be operated simultaneously. The applied input voltage is 1 V peak-to-peak at a frequency of 500 Hz. The input AC voltage on consecutive electrodes is phase-shifted by 90 degrees. This produces a traveling wave potential having a wavelength of 160 μm and 240 μm. Each electrode in the set is driven with an input AC voltage when it is operated and the electrodes in other sets are grounded. The set1 consists of a 12 electrodes and these are 20 μm wide and separated by a distance of 40 μm. Initially, the fluid flow velocity across the outlet of the micro-pump is 32 μm/s approximately, when the set1 is operated. The fluid velocity is increased from 32 to 107 μm/s as per the requirements by switching the input voltage from set1 to set4. The insulin delivery is auto-regulated by switching the voltage between the four sets according to the glucose concentration levels.

1.4 Organization of the Thesis

The work presented in this thesis has been organized as follows. In chapter 1, we have presented introduction and motivations of our research work; additionally, an overview of thesis contributions are presented in this chapter. Chapter 2 includes the design of a microbridge for glucose sensing application. Simulation results of mechanical and electrical response of a piezoresistor based microbridge are discussed. Chapter 3 presents the basics of osmosis principle and the design details of osmotic pressure sensor. Subsequently, the simulation results of an osmotic pressure sensor is discussed. And the fabrication and packaging of a piezoresistive pressure sensor are explained in chapter 4. The experimental setup and testing of an osmotic pressure sensor is presented in Chapter 5. In chapter 6, the design of an AC electro-osmotic pump and the simulation studies are discussed. Finally, conclusion and future direction of research work are included in chapter 7.

2

Design of a micro-bridge for Glucose Sensing Application

Contents

2.1 Introduction

Advances in the field of micro-machining technology has helped fabrication of microstructures, such as bridges and microcantilevers. The unique characteristic of a microcantilever or a micro-bridge is that it bends when the molecular adsorption by confined to one side of the surface [24, 26, 27]. The enzyme glucose oxidase (GOx) based micro-machined silicon (Si) cantilever has been fabricated and demonstrated successfully for glucose detection [13, 28, 29]. The micro-bridge could be developed as a potential device for the continuous monitoring of glucose levels. Moreover, it provides the selective detection of glucose if the GOx was immobilized on

the top surface of the micro-bridge [13]. The adsorption induces a differential surface stress which causes bending in the micro-bridge. The use of micro-bridges in the development of miniaturized sensors offers advantages such as high sensitivity and the ability to work in air, liquid, harsh environments and even in a mobile working environment [24, 30]. The main challenge associated with the microcantilever is its stability in a mobile working environment and this issue can be resolved to a certain extend by the usage of micro-bridge because of its two ended support. All these advantages of micro-bridge come at the expense of lower sensitivity and low $\Delta R/R$ values compared to microcantilevers.

Micro-bridges have been fabricated using silicon (Si), silicon carbide (SiC), silicon nitride (Si_3N_4), metals, metal composites and polymers [24]. The bending of a Si micro-bridge made up of Si is very small because the adsorption induced surface stress is very small and Si material has a relatively large Young's modulus that resists the bending. The materials with smaller Young's modulus would be a more appropriate for developing chem/biosensors based on the deformation. The bending in the micro-bridge can be measured with different methods such as optical, electrostatic, piezoelectric and piezoresistance [24, 28, 31]. In this work piezoresistive sensing technique is employed. Piezoresistance based micro-bridges are becoming increasing popular in recent years as they are convenient to calibrate, readily deployable into integrated electromechanical system and do not require external detection devices.

Yanqing Lu et.al. designed and fabricated the SiO_2 based piezoresistive micro-bridge. A thin layer of P-type boron doped Si is used as the piezoresistive material to measure the bending of the SiO_2 micro-bridge [24]. In this chapter, we have designed a micro-bridge for glucose sensing application. SiO_2 is chosen as the material for the micro-bridge. The Young's modulus of SiO_2 is 76.5-97.2 GPa, which is smaller than that of Si at 155.8 GPa [32]. The SiO_2 micro-bridge is also useful in the detection of hydrogen fluoride (HF) and nerve agents as suggested in the literature [24, 30, 33, 34]. The micro-bridge employed in this work differs from the existing literature in the following ways. The two piezoresistors are placed at the edges of the micro-bridge instead of single piezoresistor along the micro-bridge [24]. The reason is that the maximum stress is at the edges compared to the middle. Moreover, the top surface of the micro-bridge can be used

for the adsorption of molecules instead of bottom surface. The deposition of active layer on top surface is very easy compared bottom surface. Additionally two more piezoresistors are placed on the anchor region of the micro-bridge where the stress is zero as shown in Fig. 2.1. This can be used as reference resistors. These four resistors are arranged in the Wheatstone bridge configuration. Compared to a single resistor scheme the output voltage of the Wheatstone bridge configuration becomes double because of the resistance changes in opposite sides. FEM is used to analyze the electrical and mechanical response of a piezoresistor based micro-bridge. The sections of this chapter are as follows. The design details of micro-bridge are explained in section 2.2. Simulation results of mechanical and electrical response of a piezoresistor based micro-bridge are given in section 2.3 and finally the chapter is summarized in section 2.4.

2.2 Design of SiO_2-based Piezoresistive micro-bridge

A micro-bridge can be constructed in a SOI substrate by etching the bulk Si using the DRIE technique as shown in Fig. 2.1. The Si under the SiO_2 micro-bridge at the two ends is used as the anchor to provide the support. In general, biomedical sensors are based on measuring the mechanical deformation caused in a micro-bridge or membrane when it experiences the stress due adsorption induced differential surface stress. The fixed end beam is subjected to a surface stresses σ_s^+ and σ_s^- on upper and lower surfaces, respectively as shown in Fig. 2.2(a). The surface stress effects are considered as uniformly distributed forces on the top surface of the micro-bridge [35] and its units are N/m. Fig. 2.2(b) shows the beam with uniformly distributed load along the x-direction. Euler-Bernoulli beam theory is used to describe the beam bending. The beam ends are fixed and a uniformly distributed load is considered to solve the beam deflection from the fourth-order differential equation of a simple beam theory as follows [36].

$$EI\frac{d^4w(x)}{dx^4} = -q \tag{2.1}$$

where E is the Young's modulus, I is the moment of inertia and q is the load in N/m. For the rectangular beam, $I = b \cdot h^3/12$, b and h are the micro-bridge width and thickness, respectively.

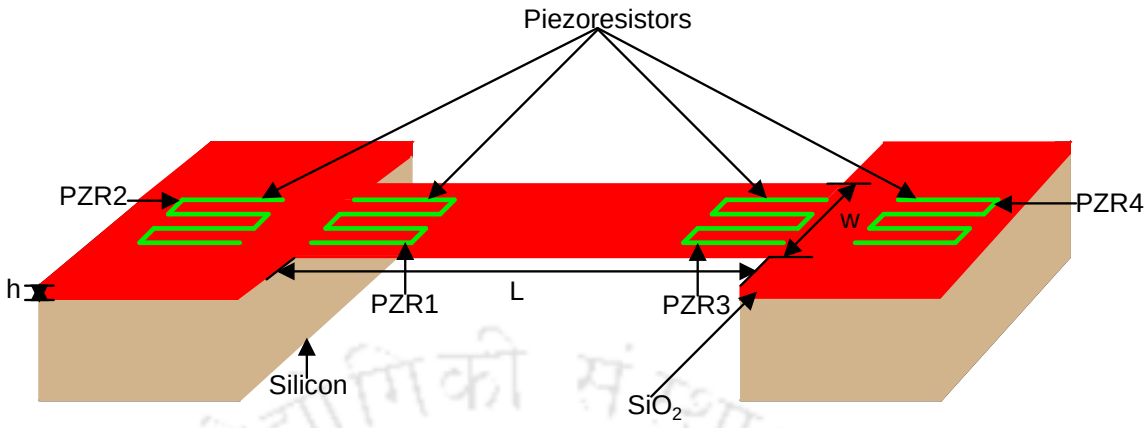

Figure 2.1: The SiO_2 micro-bridge with P-type piezoresistors on the top surface.

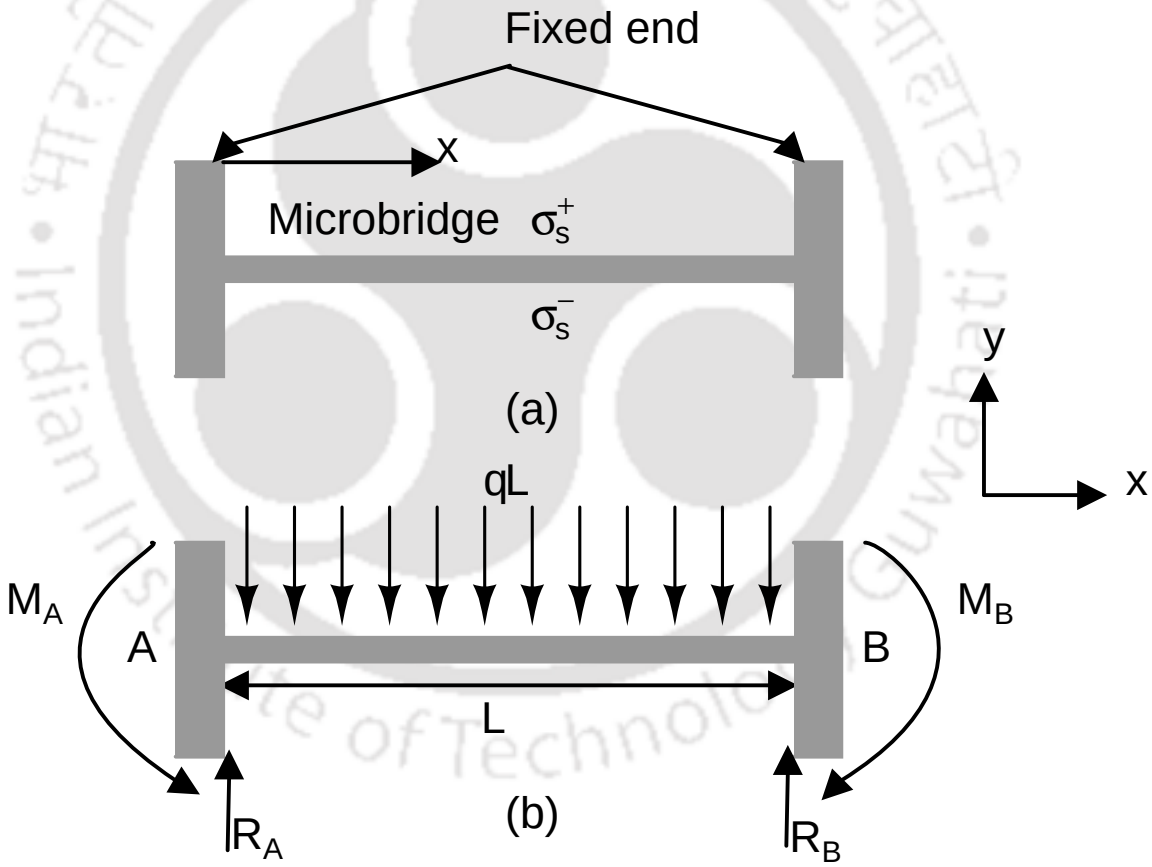

Figure 2.2: The fixed end beam with uniformly distributed load q.

The load on this beam acts only in the vertical direction, hence there are no horizontal reaction forces at the supports. The reaction forces and bending moments at the support A and B are $R_A = R_B$ and $M_A = M_B$, respectively because of symmetry of the beam. The reaction force R_A

$= R_B = \mathrm{q}\cdot\frac{L}{2}$ since the vertical reaction forces are equal. The successive integration of equation (2.1) gives the shear forces, bending moments, slope and deflections of the beam.

$$E \cdot I \cdot \frac{d^3w(x)}{dx^3} = -q \cdot x + c_1 \tag{2.2}$$

$$E \cdot I \cdot \frac{d^2w(x)}{dx^2} = -\frac{q \cdot x^2}{2} + c_1 \cdot x + c_2 \tag{2.3}$$

$$E \cdot I \cdot \frac{dw(x)}{dx} = -\frac{q \cdot x^3}{6} + c_1 \cdot \frac{x^2}{2} + c_2 \cdot x + c_3 \tag{2.4}$$

$$E \cdot I \cdot w(x) = -\frac{q \cdot x^4}{24} + c_1 \cdot \frac{x^3}{6} + c_2 \cdot \frac{x^2}{2} + c_3 \cdot x + c_4 \tag{2.5}$$

The boundary conditions for a fixed end beam are given as

$$w(0) = 0, \quad \frac{dw(0)}{dx} = 0, \quad \frac{dw(\frac{L}{2})}{dx} = 0 \tag{2.6}$$

where L is the length of the micro-bridge along the x-direction. The five unknown constants c_1, c_2, c_3, c_4, and M_A are obtained by substituting the boundary conditions into the above equations (2.2)-(2.5). When these five constants are substituted in equation (2.5), the deflection of the micro-bridge is obtained.

$$c_1 = q \cdot \frac{L}{2},\ c_2 = -M_A,\ C_3 = C_4 = 0,\ M_A = q \cdot \frac{L^2}{12} \tag{2.7}$$

$$w(x) = -\frac{q \cdot x^2}{24 \cdot E \cdot I} \cdot (x^2 - 2 \cdot L \cdot x + L^2) \tag{2.8}$$

The differential surface stress $\Delta\sigma$ ($\Delta\sigma = \sigma_s^+$ - σ_s^-) causes deflection in the micro-bridge. However, the stress is maximum at the edges, in practice, the stress is not uniformly distributed. The maximum deflection in the micro-bridge is at $x = \frac{L}{2}$ and it is given by.

$$w = -q \cdot \frac{L^4}{32 \cdot E \cdot b \cdot h^3} \tag{2.9}$$

The deflection in micro-bridge is measured in terms of change in the resistance of piezoresistors which are formed on the top layer of Si as shown in Fig. 2.1. The piezoresistors are made up of a boron-doped Si (P-type), because its sensitivity is more compared to an N-type Si. The advantage of using piezoresistor is that it provides a linear variation in resistance for the stress

being measured and is simple to fabricate. Finite Element Modeling analysis is performed to study the deformation, stress and the change in resistivity of a piezoresistive material by applying the external force on the top surface of the micro-bridge. The MemMech and MemPZR modules in CoventorWare are used to study the mechanical behavior of the micro-bridge and compute the change in resistivity of a piezoresistive material subject to mechanical deformations. Piezoresistivity in Si arises from the deformation of energy bands as a result of stress. The resistivity of a material depends on the internal atom positions and their motions. Ohm's Law in the stress-free state represents this effect mathematically [37].

$$\begin{bmatrix} E_1 \\ E_2 \\ E_3 \end{bmatrix} = \rho_0 \begin{bmatrix} 1 & 0 & 0 \\ 0 & 1 & 0 \\ 0 & 0 & 0 \end{bmatrix} \begin{bmatrix} i_1 \\ i_2 \\ i_3 \end{bmatrix}$$

where E_i and i_i are the electric field and current density, respectively, parallel to the x_i crystallographic axis, and ρ_0 is the stress-free resistivity. The change in resistance for the applied stress is given by the following equation (2.10).

$$R = \rho_0 \frac{L_R}{W_R \cdot t_R}, \quad \frac{\Delta R}{R} = \Pi_l \cdot \sigma_l \tag{2.10}$$

where R is the fixed resistance, t_R is the thickness of the piezoresistor, W_R and L_R are the width and length of the piezoresistor, respectively, Π is the piezoresistive coefficient of silicon, σ is the stress and the subscript l refer to longitudinal stresses with respect to the resistor axis. The stress for a micro-bridge is given in equation (2.11).

$$\sigma_l = \frac{M \cdot y}{I} \tag{2.11}$$

here M is the bending moment and y is the distance from the natural axis of a micro-bridge. The relationship between the stress and the deformation of a micro-bridge is obtained by calculating the bending moment at different values along the x-direction. The piezoresistive coefficients for the P-type Si and the material properties used in this work are listed in the table 2.1.

Table 2.1: Material Properties for the micro-bridge

Material Property	Si [1 1 0]
Young's modulus (MPa)	1.30191×10^5
Poisson's ratio	0.278
Shear modulus (MPa)	7.9624×10^4
Density (kg/μm^3)	2.32899×10^{-15}
Thermal coefficient (pW/μm K)	1.48×10^8
Resistivity (Ω-cm)	7.8
Material	SiO_2
Young's modulus (MPa)	7.0×10^4
Poisson's ratio	0.17
Piezoresistive coefficients P-type silicon	(MPa^{-1}) $\pi_{11} = 6.6 \times 10^{-5}$ π_{12} = -1.1 $\times 10^{-5}$ $\pi_{44} = 138.1 \times 10^{-5}$

2.3 Simulation Results

The main objective of the simulations is to understand the mechanical and electrical behavior of the material under the influence of the external force. This can lead to the optimization of parameters such that the design specifications are completely satisfied and the micro-bridge yields its best performance. Initially, the appropriate process steps are defined to construct a 2D layout of a micro-bridge. The next step is the extraction of 3D model from 2D layout and assigning of the boundary conditions. Meshing for the micro-bridge has been achieved using Manhattan bricks (parabolic elements). Some parts like the anchor of the micro-bridge structure, is not meshed closely so as to reduce the computational load.

The geometrical parameters of the micro-bridge are optimized. The deflection in the micro-bridge is observed by applying uniformly distributed load along the length of the micro-bridge whose two ends are fixed as shown in Fig. 2.2(b). A 2 N/m surface stress is used in this study because the surface stress changes at this level have been observed in many chem/biosensors [38]. The length has great influence on the nonlinearity and sensitivity of the micro-bridge compared to the width. Fig. 2.3(a) shows the deformation in micro-bridge at different values

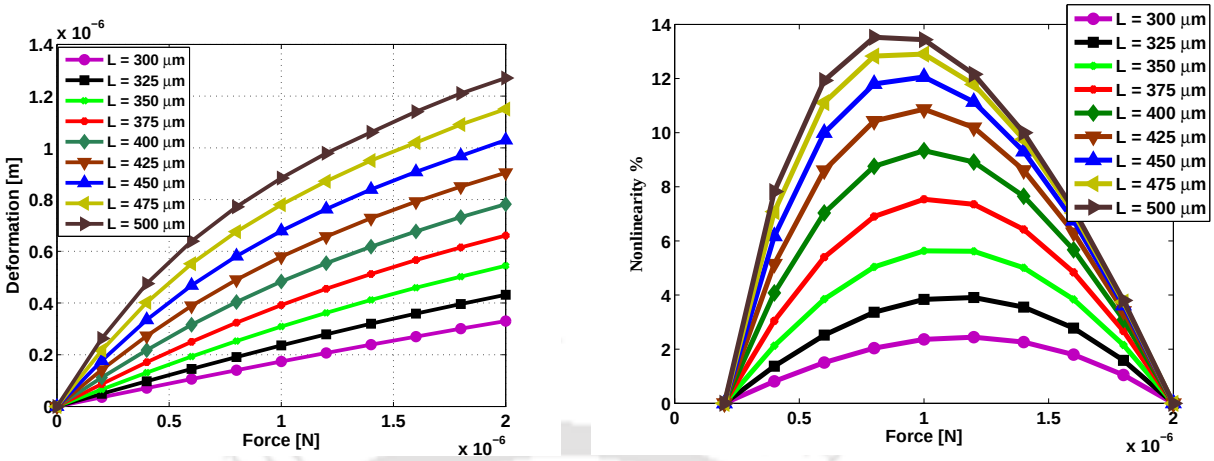

(a) (b)

Figure 2.3: Deformation and nonlinearity in the micro-bridge (a) The deformation versus force for the different lengths (b) Nonlinearity profile with respect to the deflection when the force is varied from 0 to 2 μN.

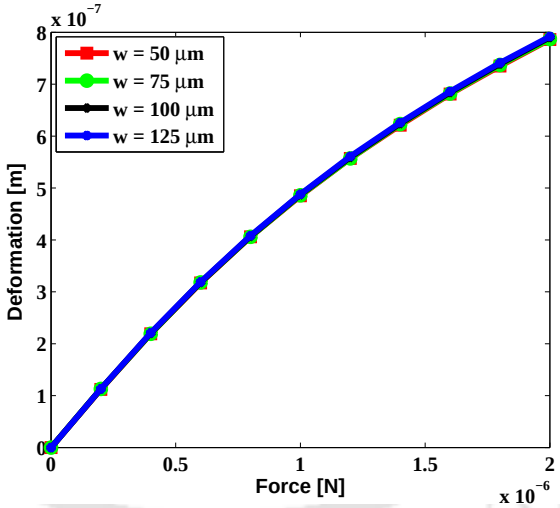

Figure 2.4: The deformation versus force for the different widths of micro-bridge when the force is varied from 0 to 2 μN.

of length at constant width when the force is varied from 0 to 2 μN. Fig. 2.3(b) shows the nonlinearity in the micro-bridge for different values of length. If the length is increased from 300 μm to 500 μm, the sensitivity increases, but the nonlinearity also increases. The nonlinearity will be minimal with smaller lengths, but one need to compromise the sensitivity at such lengths. Fig. 2.4 suggests that the variation in the width of the micro-bridge has lesser impact

on nonlinearity as well as sensitivity.

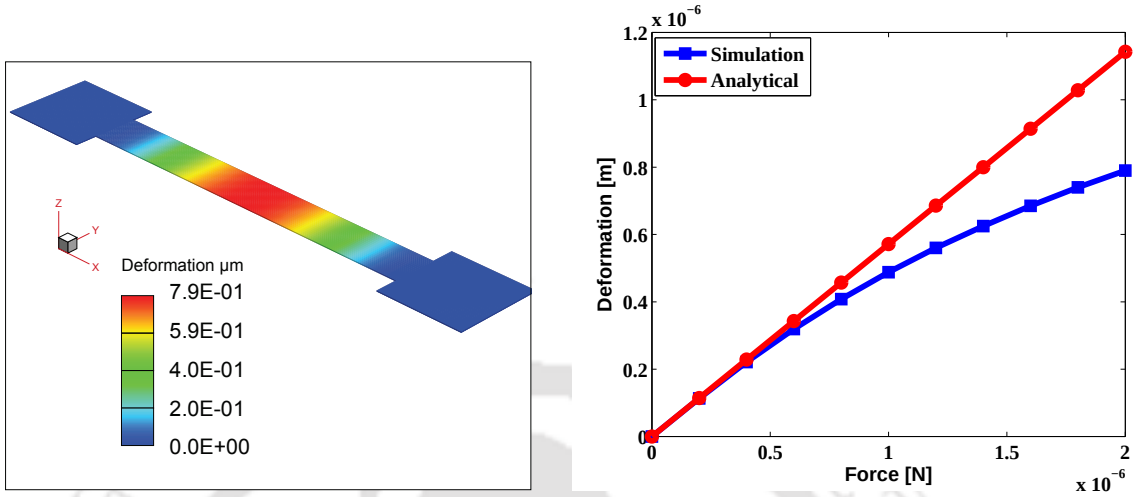

(a) (b)

Figure 2.5: Deformation in the SiO_2 micro-bridge (a) Maximum deformation is at center for an applied force of 2 μN (b) deformation increases as the force increases from 0 to 2 μN.

The dimensions of the micro-bridge are chosen as 400 μm x 50 μm x 1 μm by considering both the nonlinearity and sensitivity aspects. Fig. 2.5(a) shows that the maximum deformation is at the center of a micro-bridge for a force of 2 μN. The deformation of the micro-bridge is increased from 0 to 0.787 μm, when the force is increased from 0 to 2 μN, as shown in Fig. 2.5(b). Analytical and simulations results are closely matched when the force value is below 0.6 μN but as the force increases further, the error also increased to 20% as shown in Fig. 2.5(b). The stress profile in Fig. 2.6(a) suggests that the maximum stress is at the edges of the micro-bridge and the stress decreases along the x-direction towards the origin. Fig. 2.6(b) shows the stress profile along the x-direction. The maximum compressive stress is 6.00 MPa and it decreases towards the origin. The two piezoresistors are placed near the edges of the micro-bridge to measure the deformation as shown in Fig. 2.1. This will increase the sensitivity and moreover, the top surface can be used as the active layer. To study the resistance variation in the piezoresistor, the deformation and stress computed in the MemMech module are copied into the MemPZR. The sensitivity can be expressed as the change in resistance of the piezoresistor (ΔR/R) with respect to the stress being measured. The change in resistance observed at different locations along the x-direction from 5 μm to 160 μm is shown in Fig. 2.7.

The maximum value of ΔR/R is 6.15x10^{-4} which is located at 154 μm away from the origin along the x-direction. The location of the two piezoresistors is fixed so that it will experience the maximum stress in the micro-bridge. This approach would result in an increased sensitivity which is 4 times higher than the existing work [24].

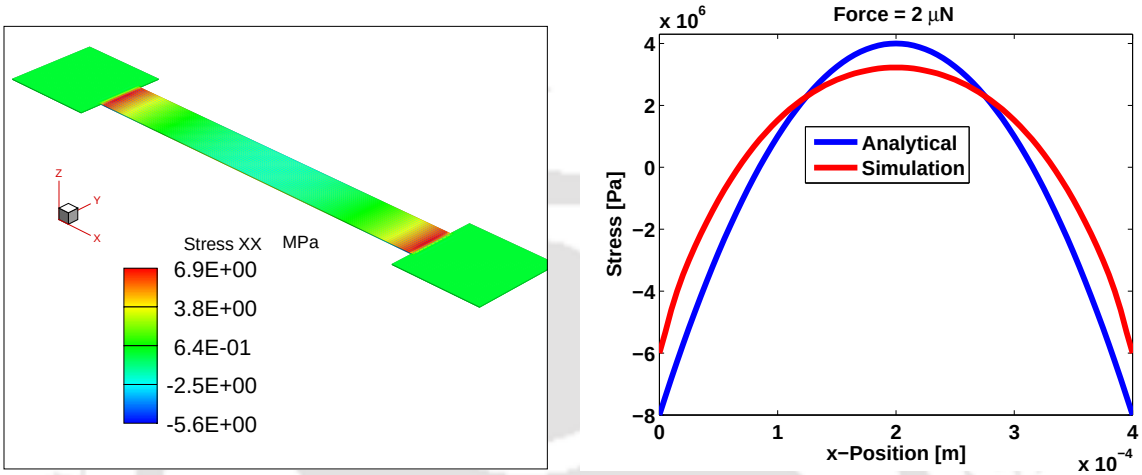

(a) (b)

Figure 2.6: (a) The maximum stress is at the edges of the SiO_2 micro-bridge when a force of 2 μN is applied (b) The stress profile in the x-direction.

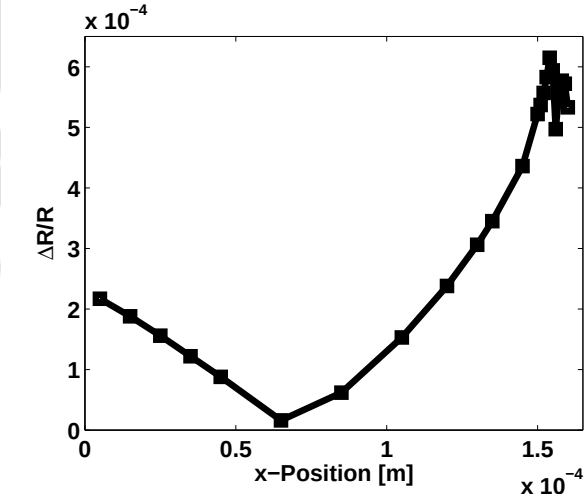

Figure 2.7: The ΔR/R of SiO_2 micro-bridge at different positions along the x-axis.

The geometrical parameters of the piezoresistors have the great influence on the sensitivity of the SiO_2 micro-bridge. Fig. 2.8(a) shows that the deformation increases as the thickness decreases from 2 μm to 0.2 μm, when a 2 μN force is applied on the surface of the micro-bridge.

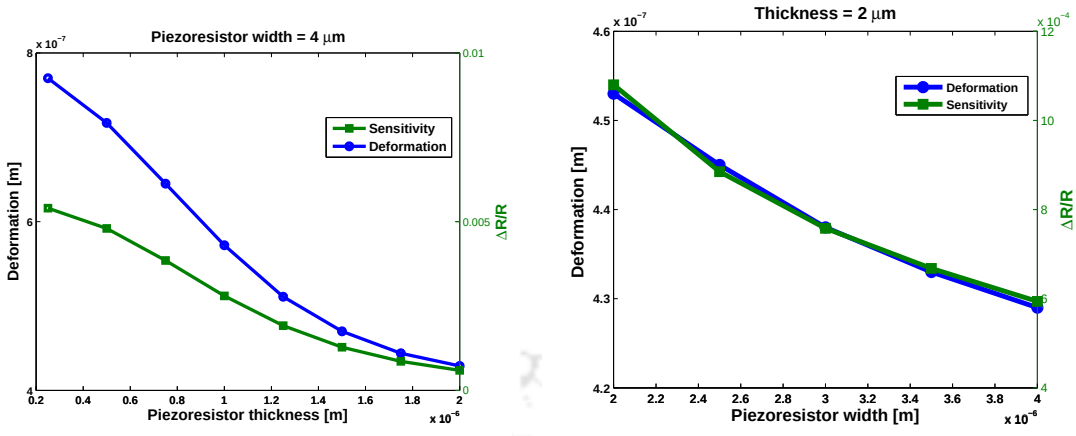

(a) (b)

Figure 2.8: (a) The deformation and $\Delta R/R$ of the SiO_2 micro-bridge versus the thickness of the Si piezoresistors (b) The deformation and $\Delta R/R$ of the SiO_2 micro-bridge versus the width of the Si piezoresistors.

The simulation results in Fig. 2.8(a) show that deformation increases from 0.429 μm to 0.78 μm and $\Delta R/R$ increases from 0.000594 to 0.0055. If the piezoresistor thickness is very small the deformation is higher and the piezoresistor experience the larger value of stress. A decrease in width from 4 μm to 2 μm, increases both the deformation and the sensitivity. The deformation is increased from 0.429 μm to 0.453 μm and $\Delta R/R$ increases from 0.000594 to 0.00108, when a 2 μN force is applied on the surface of the micro-bridge as shown in Fig. 2.8(b). The thickness of the piezoresistors has a more significant effect on the sensitivity of the micro-bridge compared to the width of the piezoresistor, though both can affect the deformation as well as the $\Delta R/R$ of micro-bridge as shown in Fig. 2.9(a) & 2.9(b). The maximum change of $\Delta R/R$ is 0.00568 for a width of 2.5 μm and a thickness of 0.25 μm piezoresistors. The placing of piezoresistors on the micro-bridge and the optimization of the geometrical parameters of the piezoresistors is expected to result in the improved performance. Finally, the change in resistance of the piezoresistors is converted to voltage by arranging the four resistors in the Wheatstone bridge configuration as shown in Fig. 2.10. The resistances of the two piezoresistors PZR1 and PZR3 vary according to the differential surface stress on the micro-bridge as shown in Fig. 2.1. The PZR2 and PZR4 are used as reference resistors and their resistances will not change.

The small variation in the resistance of piezoresistors as the result the differential surface

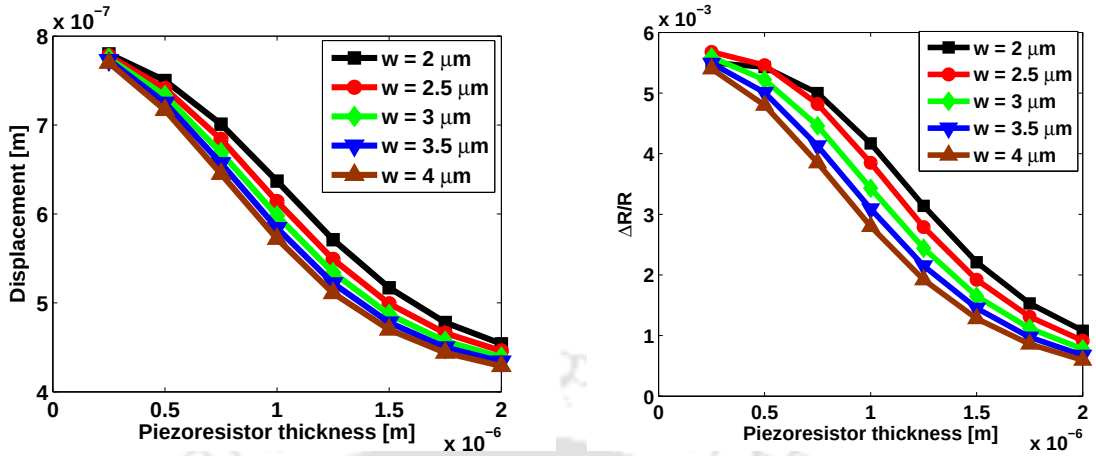

(a) (b)

Figure 2.9: (a) The deformation and (b) $\Delta R/R$ of the micro-bridge versus the thickness of the Si piezoresistors, when the width is varied from 2 μm to 4 μm.

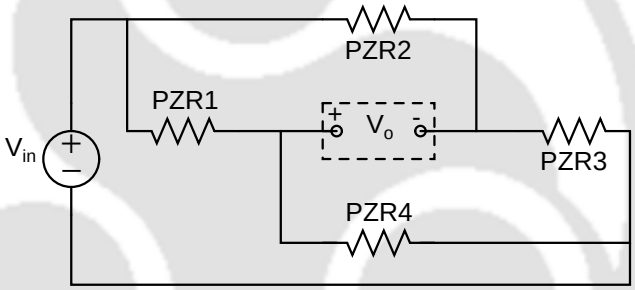

Figure 2.10: Wheatstone bridge configuration of 4 piezoresistors.

stress on the micro-bridge can be observed in terms of output voltage. For the different values of the input voltages, the change in output voltage of the SiO_2 micro-bridge is shown in Fig. 2.11(a). The change in output voltage of the SiO_2 micro-bridge is from 0 to 1.472 mV, when a force value is varied from 0 to 2 μN. The relationship between the output voltages with respect to the force is linear as shown in Fig. 2.11(b). The output voltage obtained is twice since the change in resistance of two piezoresistors is considered instead of single piezoresistor.

2.4 Summary

A SiO_2 micro-bridge was designed and simulated to measure the small variation of surface stress on the micro-bridge. The mechanical behavior of the SiO_2 micro-bridge was studied

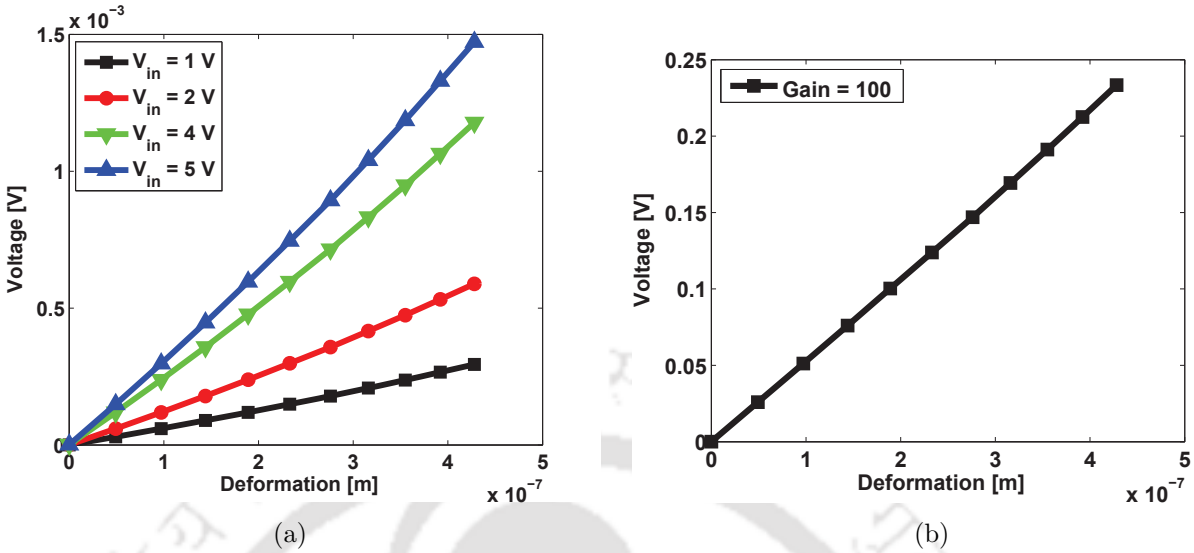

(a) (b)

Figure 2.11: Deformation verses the output voltage of the SiO_2 micro-bridge (a) Input voltage is varied from 1 V to 5 V (b) Input voltage is 5V and Gain is 100.

using the FEM and the dimensions for the micro-bridge are optimized. The stress profile and the deformation of micro-bridge were analyzed. The piezoresistors were placed at the edges of the micro-bridge to experience the maximum stress. The effect of geometrical parameters of piezoresistors on the sensitivity of the micro-bridge was studied. The changes in resistance of the piezoresistors were measured in terms of change in voltage by arranging the piezoresistors in Wheatstone bridge configuration. The output voltage obtained was twice since the change in resistance of two piezoresistors was considered instead of single piezoresistor. Output voltage of the SiO_2 micro-bridge was from 0 to 1.472 mV, when a force value was varied from 0 to 2 μN, without any amplification of the output voltage.

3

Design and Simulation of an Osmotic Pressure Sensor

Contents

3.1 Introduction

Different kinds of microelectromechanical systems (MEMS) devices have been designed for potential biomedical applications such as pressure sensing, diagnostic monitoring and drug delivery. Various kinds of stored energies like electrical, electrochemical, mechanical, and chemical energy [39, 40, 41, 42] can be exploited to produce mechanical actuation in MEMS devices. Osmosis is a natural phenomena and the osmotic energy employed in an osmotic microactuator, has been demonstrated successfully to provide a mechanical actuation [19]. This mechanism is the basis for the development of many kinds of osmotic pumps which may be used to provide

a controlled drug delivery without consuming any electrical energy[17, 20, 25]. Further, the osmosis principle is extended for the measurement of osmotically active substance in the body fluid [16]. However, these devices suffer from poor values of sensitivity and response time, and larger system size [18]. Moreover, most of the osmotic sensors employs a polymer material which limits the integration of an electronic circuit needed to monitor the external glucose concentration levels [17].

Analytical and numerical simulations on the microactuators have been previously presented by different researchers [43, 44]. Modeling and simulation of MEMS devices are of vital importance in developing innovative products at reduced fabrication cost and time. Advanced design methodologies and a variety of software tools are needed to analyze the mechanical, electrical and fluidic behaviors in systems. The computer simulations provide understanding of the device behavior and help to optimize the geometrical parameters and improve the performance of the structure. MEMS devices are popularly analyzed using FEM (Finite Element Method) or BEM (Boundary Element Method) or FVM (Finite Volume Method), to solve related partial differential equations. The design and simulation of MEMS are inherently complex in nature. The realization of complete system behavior is even more complex if the MEMS structures are integrated with microfluidic devices.

In this chapter, we have focused on the design and simulation aspects of an osmotic pressure sensor. To the best of our knowledge there are no simulation reports available for the osmotic pressure sensor based on the FEM and FVM. The FEM is used for the electro-mechanical analysis of pressure sensor and the FVM is employed for the fluid flow analysis across a porous medium. The Si material is chosen for the device instead of a polymer material. The advantage of using the Si material over the polymer material is that the electronic circuit can be integrated on the same substrate. The osmotic pressure sensor consists of a square cavity on the bottom side to fill the osmotically active substance. The filled cavity is sealed with a semi-permeable membrane. The solvent moves in/out of the device if there is any change in concentration difference across the semi-permeable membrane. The in/out solvent flow across creates a volume change inside the device cavity which causes the displacement in the Si membrane. Further,

the piezoresistors are diffused onto the top side of a Si membrane and these are arranged in a Wheatstone bridge configuration to facilitate the measurement of stress. The sections of this chapter are as follows. The basics of osmosis principle and the design details of osmotic pressure sensor are explained in section 3.2 and 3.3 respectively. Simulation results of an osmotic pressure sensor is discussed in section 3.4 and finally the chapter is summarized in section.

3.2 Osmosis Principle

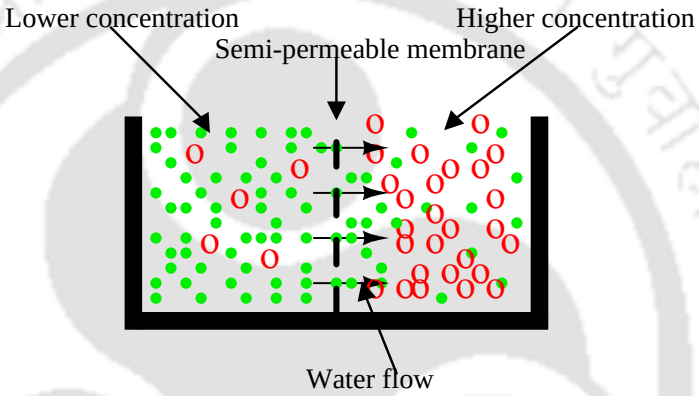

Figure 3.1: Water transportation across semi-permeable membrane.

Osmosis is a natural phenomena and it is a passive transport mechanism widely found in a variety of biological systems [15]. It is defined as the net movement of solvent flow across a semi-permeable membrane driven by a difference in concentration levels as shown in Fig. 3.1. The semi-permeable membrane separates a solution of lower concentration (on the left side) from a solution of higher concentration (on the right side) in a vessel. The smaller solid circles indicate water molecules and the bigger hollow circles indicate solute molecules (ions) like sugar and urea. There are two different osmosis mechanisms described as forward osmosis (FO) and reverse osmosis (RO). In RO, the applied pressure is the driving force for the flow of solvent through membrane, unlike in FO, the osmotic pressure itself is the driving force for the mass transport [45]. The osmotic pressure is related to the concentration of solute particles and a mathematical relationship is formulated by Van't Hoff [46]. The osmotic pressure due to the solute concentration is given in equation (3.1).

$$\Delta\pi = RT\Delta C \tag{3.1}$$

where ΔC is the concentration difference, R is the gas constant and T is the temperature. Due to the concentration difference, an osmotic pressure develops and the water molecules move from lower concentration region to higher concentration region as indicated by arrows. The ideal semi-permeable membrane allows only the passage of water but rejects the large size solute molecules (ions). Equation (3.2) describes the rate of solvent flow through the semi-permeable membrane [25].

$$J_v = \frac{K_p}{\eta d_m} A(\sigma\Delta\pi - \Delta P) \tag{3.2}$$

where K_p is the filtration coefficient, J_v is the volume flow of solvent per unit time, A is the surface area of the membrane, σ is reflection coefficient of membrane, η is the dynamic viscosity of the fluid, d_m is the thickness of the semi-permeable membrane, $\Delta\pi$ and ΔP are the differences in osmotic and hydrostatic pressure respectively.

3.3 Design of an Osmotic Pressure Sensor

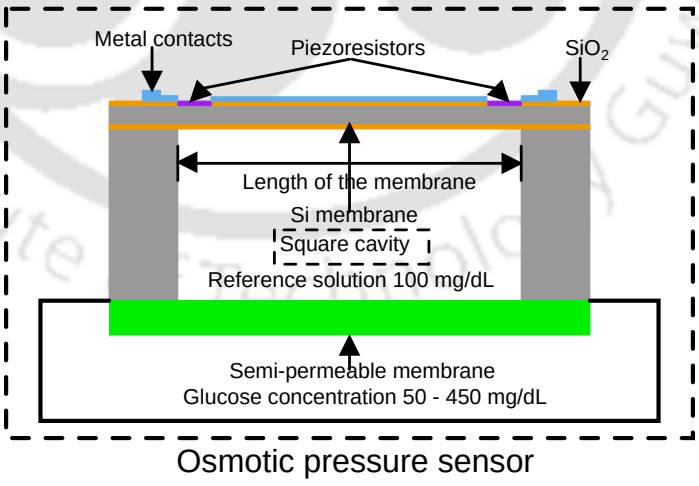

Figure 3.2: Osmotic pressure sensor based on osmosis principle.

Fig. 3.2 shows the schematic diagram of an osmotic pressure sensor. The device consists of an actuation membrane on the top side and it is formed on a SOI substrate by making the

square cavity on the bottom side. The square cavity used to fill the reference solution and sealed with a semi-permeable membrane. The osmotic pressure sensor measures the change in glucose concentration levels outside with respect to the reference solution of 100 mg/dL.

The solvent will pass through the semi-permeable membrane if there is any change in glucose concentration outside. The flow of solvent through the semi-permeable membrane is controlled by different parameters such as a $\Delta\pi$, σ, K_p and area of the membrane. $\Delta\pi$ is related to concentration difference across the semi-permeable membrane. σ defines the amount of solute particles passed through the membrane in/out. Ideally, σ is equal to unity which means that semi-permeable membrane will reject all the solute particles except water from passing through. The filtration coefficient or permeability of the semi-permeable membrane is related to the geometrical parameters such as molecular weight cut off (MWCO) and thickness. The permeability of the membrane depends on the geometrical parameters and is determined using the CarmanKozeny equation [47].

$$K_p = \frac{d_p^2 \phi^2}{180(1-\phi)^2} \tag{3.3}$$

where d_p is the particle diameter and ϕ is the porosity. The geometrical parameter of the semi-permeable membrane are chosen such that it only allows the solvent to pass through and not the solute. The pore diameter is from 5 Å to 10 Å, which is greater than water molecule diameter of 3.8 Å [48]. The size of the glucose molecule is approximately 9 Å and therefore membrane allows only water not the solute. The membrane thickness varied from 120 μm to 200 μm approximately. Permeability varies from 8.53×10^{-21} m^2 to 7.65×10^{-19} m^2 approximately.

Once the geometrical parameters of the semi-permeable membrane are fixed, the initial flow rate is determined by the particular concentration difference. The in/out flow of solvent through a semi-permeable membrane creates a volume change inside the cavity and leads to the deflection of a Si membrane on the top side. The deflection in the Si membrane is high because of the fact that semi-permeable membrane is stiff and thickness is high. The displacement in the Si membrane is linearly proportion to the Volume change in the device cavity. The relation between the volume change and the displacement are obtained by the integration of

bending envelope of a Si membrane. The bending and the volume change are given by equations (3.4), (3.5) respectively. All the equations are for the square cavity structure and based on the assumption that the pressure (P) is uniformly distributed on the top surface of a Si membrane, and fixed at four edges as shown in Fig. 3.3.

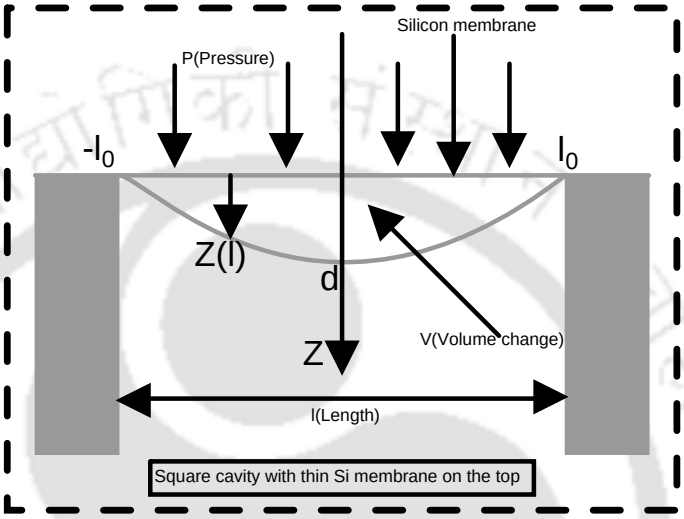

Figure 3.3: Cross sectional view of the square cavity and pressure is uniformly distributed on surface of the membrane.

$$Z(l) = w\left[1 - \left(\frac{l}{l_o}\right)^2\right]^2 \tag{3.4}$$

$$V = \int_0^w l^2 wz = l_0^2 \int_0^w \left(1 - \sqrt{\frac{z}{w}}\right) wz = \frac{l_0^2}{3} w \tag{3.5}$$

where $Z(l)$ is the bending in the membrane, w is the displacement, V is the volume change and the l_0 is the half of side length of the membrane. The rate of change of displacement in the Si membrane for the change in glucose concentration as the function of time is obtained by substituting equation (3.2) in (3.5) and it is given by equation (3.6).

$$\frac{\Delta w}{\Delta t} = \frac{12}{l^2}\left(\frac{K_p}{\eta d_m} A(\sigma \Delta\pi - \Delta P)\right) \tag{3.6}$$

where w is the displacement and t is the response time. The solvent flow across the semi-permeable membrane in/out exert a pressure on the surface of a Si membrane and it is measured

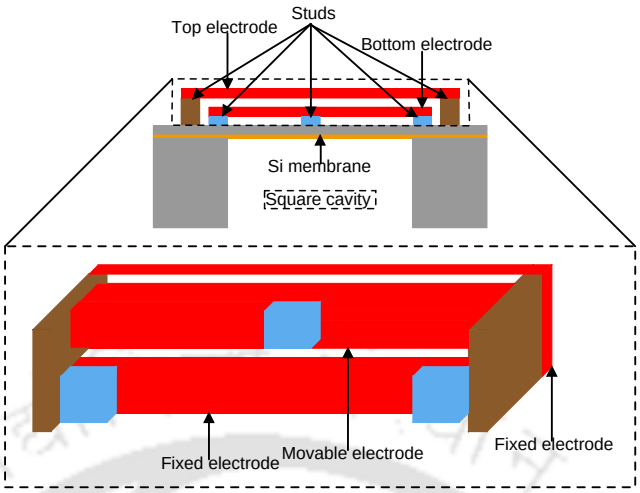

Figure 3.4: Capacitive pressure transducer.

in terms of displacement. The relation between pressure and displacement of a Si membrane is given by equation (3.7) [49].

$$\Delta P = \frac{16Eh^4}{l^4}\{\frac{4.2}{1-\nu^2}(\frac{\Delta w}{h}) + \frac{1.58}{1-\nu}(\frac{\Delta w}{h})^3\} \tag{3.7}$$

where E is Young's modulus, ν is Poisson's ratio, h is the thickness of the membrane, P is the pressure, and l is the length of the membrane.

3.3.1 Different Types of Sensing Techniques

Three different sensing techniques such as capacitive, piezoelectric and piezoresistance are studied to measure the displacement in the Si membrane of the osmotic pressure sensor.

3.3.1.1 Capacitive Pressure Transducer

The capacitive sensor is the first choice to measure the displacement of the membrane. The capacitance, C of a parallel plate capacitor is given by equation (3.8).

$$C = \frac{A_p \epsilon_0 \epsilon_r}{d} \tag{3.8}$$

where A_p is the area of overlap of the two plates, ϵ_r is the relative permittivity, ϵ_0 is the permittivity of free space and d is the separation between the plates. A parallel plate capacitor

consists of two electrodes, bottom and top electrode. The top electrode is fixed and attached to the side walls of the device with studs. The bottom electrode is split into two parts, fixed and movable as shown in Fig. 3.4. The fixed electrode is attached to anchor region of the device with studs. The movable electrode is attached to the center of the membrane with a single stud where maximum displacement occurs. Here, the advantage is that among two capacitances, one is variable and another is fixed. In the case of small dimensions where the variation expected is very small, this kind of structure is very helpful. Even if the variable capacitance variations are small compared with the fixed capacitance it can be sensed by using a differential amplifier principle. The change in the capacitance due to the displacement in the membrane is given by equation (3.9).

$$C = \frac{A_p \epsilon_0 \epsilon_r}{d_0 + d_z} \tag{3.9}$$

Here d_0 is the initial gap between the plates and d_z is the gap between the plates due to displacement.

The advantage of capacitive sensor is that it is temperature independent and it has better sensitivity. The ratio of change in capacitance to fixed capacitance may be improved by appropriate geometrical parameters. However, the capacitance variation is not linear and when the displacement between the capacitor plates increases, the nonlinearity also increases. An additional sophisticated interface/compensation circuit is required to sense the very small variations in capacitance [50]. Moreover, the fabrication of parallel plate capacitor on the Si membrane requires complex process.

3.3.1.2 Piezoelectric Pressure Transducer

The piezoelectric materials translate mechanical energy to electrical energy and vice versa. This basic principle may be used for applications such as pressure sensor, actuation and vibration control. In the present work, a piezoelectric based, multilayered membrane is used to measure the osmotic pressure inside the cavity. The membrane can be constructed from a Si substrate by using bulk micro-machining followed by deposition of Si nitride (Si_3N_4), titanium (Ti), platinum (Pt), piezoelectric material (ZnO) and Pt layers as shown in Fig. 3.5. The

piezoelectric material works as a sensing material because its electrical potential changes when it experiences strain due to applied pressure.

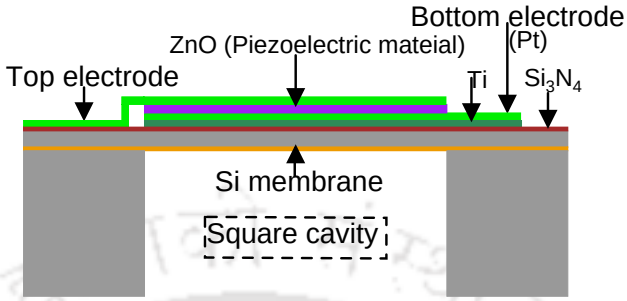

Figure 3.5: Piezoelectric pressure transducer.

In this case, an additional electronic circuit is not required because of the pyroelectric effect, by which a material generates an electric potential in response to a pressure change. The fabrication is simple compared to capacitive sensor. The sensitivity is smaller and it is also temperature dependent. Moreover, the potential change is not linear with respect to the pressure changes.

3.3.1.3 Piezoresistive Pressure Transducer

Piezoresistivity is the dependence of electrical resistivity on strain. The displacement in Si membrane is measured in terms of change in resistance. The sensor contain sensing elements (piezoresistors) made up of a P-type Si because its sensitivity is more compared to an N-type silicon. As shown in Fig. 3.6 piezoresistors are buried in a square Si membrane using a boron diffusion process. The resistivity of a material depends on the internal atom positions and their motions. These resistors are arranged in a Wheatstone bridge configuration to sense the stress in the membrane caused by the pressure being measured. The change in resistance for the applied stress is given by equation (3.10).

$$R = \rho_0 \frac{L_R}{W_R t_R}, \quad \frac{\Delta R}{R} = \Pi_l \sigma_l + \Pi_t \sigma_t \tag{3.10}$$

where R is the fixed resistance of the piezoresistor, t_R is the thickness of the piezoresistor, W_R and L_R are the width and length of the piezoresistor, respectively, Π is the piezoresistive

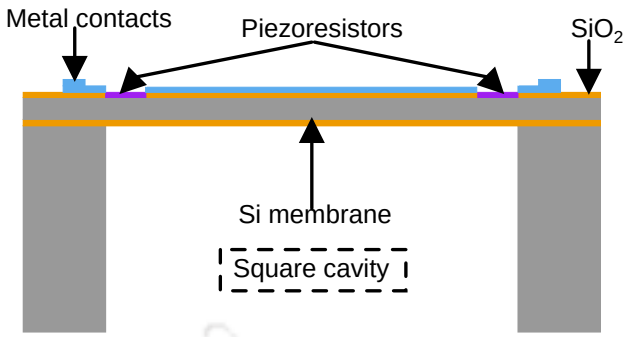

Figure 3.6: Piezoresistive pressure transducer.

coefficient of Si, σ is the stress and the subscripts l and t refer to longitudinal and transverse stresses with respect to the resistor axis.

In the bulk micro-machined structure, all resistor axes are along one of the <110> directions, and are aligned along the axis of principle stress developed at the edge of the plate. The resistor R_1 (R_3) experiences the longitudinal stress, and R_2 (R_4) experiences transverse stress. The total change in resistance for R_1 and R_2 is given by equation (3.11) and (3.12) [51].

$$\frac{\Delta R_1}{R} = (\Pi_l + \nu\Pi_t)\sigma_l \tag{3.11}$$

$$\frac{\Delta R_2}{R} = (\nu\Pi_l + \Pi_t)\sigma_l \tag{3.12}$$

where ν is Poisson's ratio having a minimum value in [110] direction of a (100) plane, with a value of 0.064 [52]. The maximum stress is at centre of membrane edge. The stresses along x and y directions are given by equation (3.13).

$$\sigma_x = 0.294(l/h)^2, \sigma_y = \nu\sigma_x \tag{3.13}$$

where l is the length of the membrane and h is the thickness of the membrane. The doping concentrations affect the piezoresistive coefficient in <110> direction for P-type Si. The piezoresistive coefficients in longitudinal (π_l) and transverse (π_t) directions are 71.8 $\times$ 10^{-11} Pa^{-1} and -66.3 $\times$ 10^{-11} Pa^{-1} respectively, and these are assumed to be constant for the low

doping concentrations (<10^{17} cm^{-3}) [52, 24]. The targeted doping concentration is approximately 4×10^{18} cm^{-3}, and it is relatively high but it will reduce the temperature dependency. The output voltage of the Wheatstone bridge circuit, by considering geometry of piezoresistor and doping concentration, is given by equation (3.14).

$$\frac{V_o}{V_s} = (\pi_{44} \times 0.141)(\frac{l}{h})^2(\frac{W_R}{L_R})\Delta P \tag{3.14}$$

where π_{44} is the piezoresistive coefficient, V_o is the output voltage, V_s is the input voltage, and L_m is the length of the Si membrane.

Three different types of sensing techniques are investigated to measure the displacement in the Si membrane and their performance is summarized in Table 3.1. The piezoresistor based sensing principle is found to be suitable for the osmotic pressure sensor because of its advantages such as simple fabrication and linear variation in the resistance with respect to the stress being measured. Moreover, any additional electronic circuit is not required.

Table 3.1: Performance comparison

Sensing technique	Nonlinearity	Sensitivity	Gauge Factor	Fabrication	Temperature
Capacitive	21.36 %	0.038	91.3	Complex	Independent
Piezoelectric	19.81 %	0.0077	18.5	Simple	Dependent
Piezoresistive	0.82 %	0.054	130	Simple	Dependent

3.4 Simulation Results

Design and simulation study of an osmotic pressure sensor are important steps for optimizing its performance, cost and time. The commercially available FEM and FVM software tools are used to understand the dependency of each design parameter on the performance of osmotic pressure sensor, and finally to optimize the design. Initially, fluid flow through the semi-permeable membrane is analyzed. The semi-permeable membrane is considered as porous medium. The flow velocity through the porous medium is analyzed using the FVM tool.

When the device is exposed to the fluid outside, having the same solution but with a different concentration, an osmotic pressure difference across the semi-permeable membrane is created and it leads to the flow of solvent in/out. P1 and P2 are pressures defined at inlet and outlet respectively, and specified as the boundary conditions corresponding to glucose concentration levels across the porous medium. Other patches are defined as walls such that no fluid can flow across them. Initially, the flow rate is maximum and it depends on the $\Delta\pi$ and on the area of the membrane since the ΔP is negligible. The $\Delta\pi$ across the semi-permeable membrane has a positive effect on the flow rate. But as the time progress ΔP increases and it has a negative effect on the flow rate, eventually at a certain point both become equal and this leads to a stop of the flow of solvent through the semi-permeable membrane as per equation (3.2).

The relation between fluid and structure interactions are analyzed by coupling three different equations. The Navier-Stokes equation solves the fluid flow through the porous medium, and Arbitrary Lagrangian-Eulerian (ALE) method handles the dynamics of structural deformation. The boundary motion is specified using the equation of a moving grid. The displacement in the Si membrane is studied using the equations on theory of elasticity. The device is considered to have two subdomains i.e. fluid and solid. The Si membrane on the top of the device is solid and the square cavity on the bottom side is fluid. For the fluid structure interaction the boundary condition is specified as fluid load. The in/out flow through the semi-permeable membrane at the end of device cavity is specified as laminar. The imbalance in concentration levels across a semi-permeable membrane develops an osmotic pressure which drags the solvent from the lower concentration region to higher concentration region until the equilibrium is reached.

The material properties of Si and the piezoresistive coefficients for the P-type Si used in this work are listed in Table 3.2 [24]. The reference glucose concentration inside the device cavity is kept at 100 mg/dL. Fig. 3.7(a) shows the fluid velocity through the semi-permeable membrane when the concentration outside is 150 mg/dL. The net flow of solvent through the semi-permeable membrane creates a volume change inside the device cavity and causes the displacement in the Si membrane. The displacement is approximately 1.13 μm after 15 min when the device has the Si membrane dimensions 3 mm $\times$ 3 mm $\times$ 10 μm, as shown in Fig.

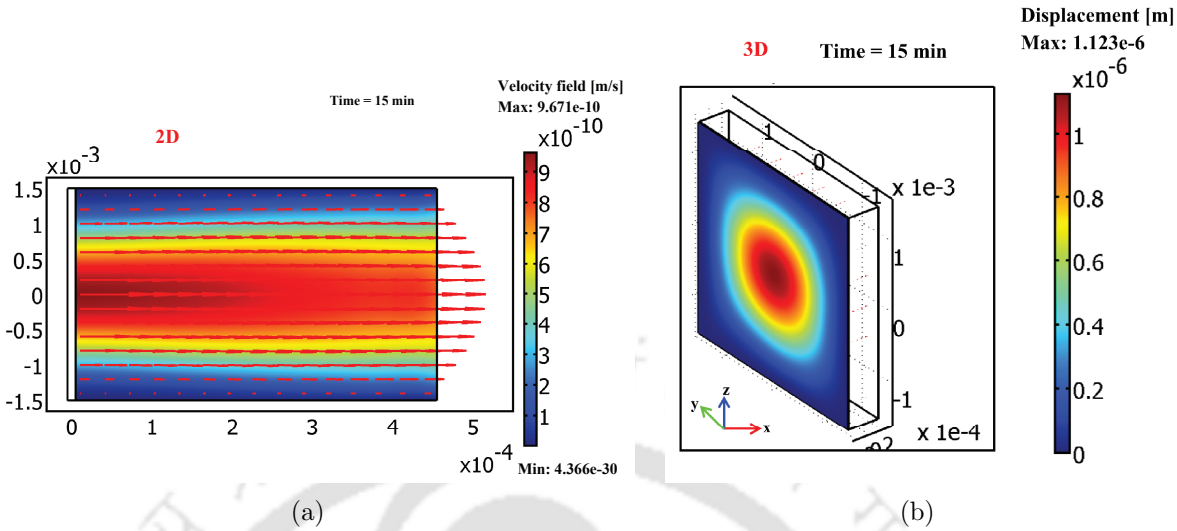

(a) (b)

Figure 3.7: (a) The relation between the fluid and structural interaction, and in the 2D plot, the arrow indicates velocity field (b) 3D plot describes the displacement in the Si membrane for a fluid load when the concentration difference is 50 mg/dL and after a time duration of 15 min.

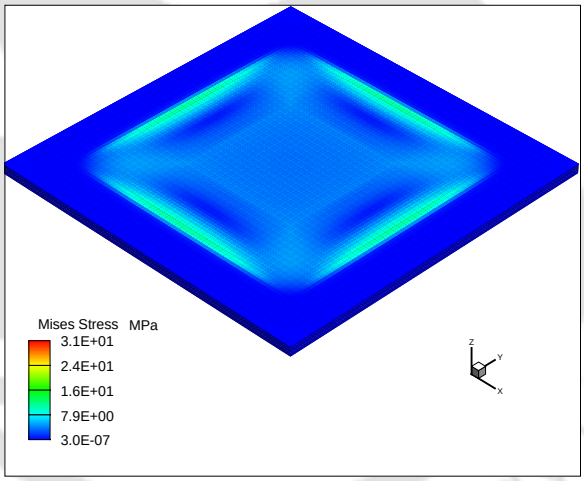

Figure 3.8: The stress is maximum at the edges of the Si membrane.

3.7(b). The displacement is maximal at the center and it is proportional to the volume change inside the device cavity. The displacement in the Si membrane increases gradually and becomes stable at one point after certain period of time, because ΔP approaches $\Delta\pi$ with time, and as a result, the volume change inside the device is not enough to push the Si membrane further. The displacement in the Si membrane introduces a stress which is maximum at the edges, as shown in Fig. 3.8. The piezoresistors are arranged in Wheatstone bridge configuration on the top of a Si membrane to measure the stress variation. The change in glucose concentration

levels from a reference value of 100 mg/dL is measured in terms of output voltage.

Table 3.2: Material Properties

Material	N-type Silicon
Young's modulus (MPa)	1.30191×10^5
Poisson's ratio	0.278
Shear modulus (MPa)	7.9624×10^4
Density (kg/μm^3)	2.32899×10^{-15}
Thermal coefficient (pW/μm K)	1.48×10^8
Resistivity (Ω-cm)	7.8
Piezoresistive coefficients P-type silicon	(MPa^{-1}) $\pi_{11} = 6.6 \times 10^{-5}$ π_{12} = -1.1 $\times 10^{-5}$ $\pi_{44} = 98.03 \times 10^{-5}$

The change in glucose concentration levels outside the device are measured with respect to the reference solution. When the device is exposed to the glucose solution of different concentration, for example 150 mg/dL, the solvent starts moves out from the device as long as the $\Delta\pi$ is higher than ΔP. The flow of solvent across the semi-permeable membrane from the device creates the volume change and this causes the displacement in the Si membrane because the of its thickness is very small compared to semi-permeable membrane thickness of 178 μm. The output voltage versus pressure for the different dimensions of the Si membrane are shown in Fig. 3.9. The output voltage across the Wheatstone bridge is increased from a 0 to 21.2 mV approximately after 40 min for a device having Si membrane dimensions are 3 mm $\times$ 3 mm $\times$ 10 μm. Initially, $\Delta\pi$ is around 6.9226 kPa approximately and ΔP is close to zero. It can be observed from Fig. 3.9 that the ΔP is increased to a 5.2 kPa and the $\Delta\pi$ is decreased which is less than 6.9226 kPa. The sensitivity is 2.10 - 1.45 mV/V/kPa when the membrane dimensions are 3.5 mm $\times$ 3.5 mm $\times$ 10 μm which is high compared to a devices having two different thickness of 10 μm and 25 μm, but having the same area of 3 mm $\times$ 3 mm as shown in Fig. 3.9.

The output voltage is linearly proportional to the ΔP when the Si membrane thickness is

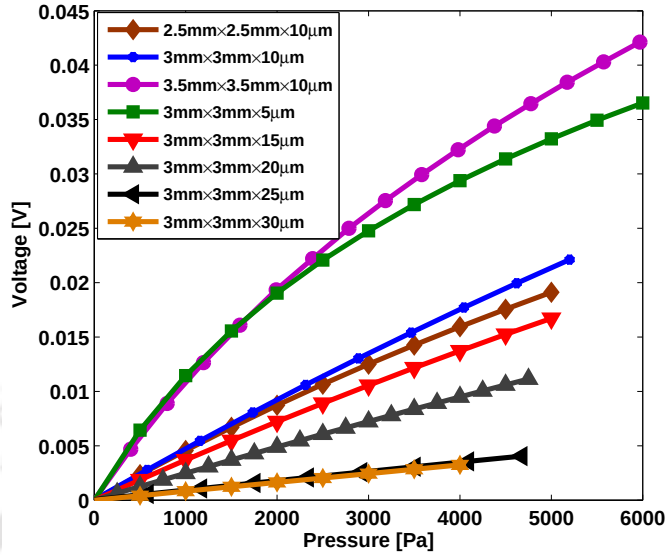

Figure 3.9: The output voltage corresponding to the glucose concentration of 150 mg/dL outside the device.

25 μm compared to 10 μm. The nonlinearity will be more if the membrane thickness is small as shown in Fig. 3.10. The nonlinearity is 12.65 % approximately for the case of device having dimensions 3.5 mm × 3.5 mm × 10 μm which is very high compared to 3.29 % and 0.82 % for the devices having two different thickness of 10 μm and 25 μm with the same area of 3 mm × 3 mm. Another limitation with decreasing the membrane thickness is that the displacement versus pressure relation equation (3.7) is not valid for the higher pressure values. So that volume change inside the cavity and displacement in the membrane is not linear at higher pressure values because of the elastic properties of material. It is good to limit the actuation displacement of a device below the Si membrane thickness. The actuation displacement and volume change are linear as long as the actuation displacement is considered to be small.

The design parameters associated with the cavity, actuation membrane, and semipermeable membrane of the pressure sensor affect the performance of the device. The response time of the device is related to the amount of volume flow across the membrane to the total volume of the device cavity. If the ratio of change in volume inside the cavity to the total volume is

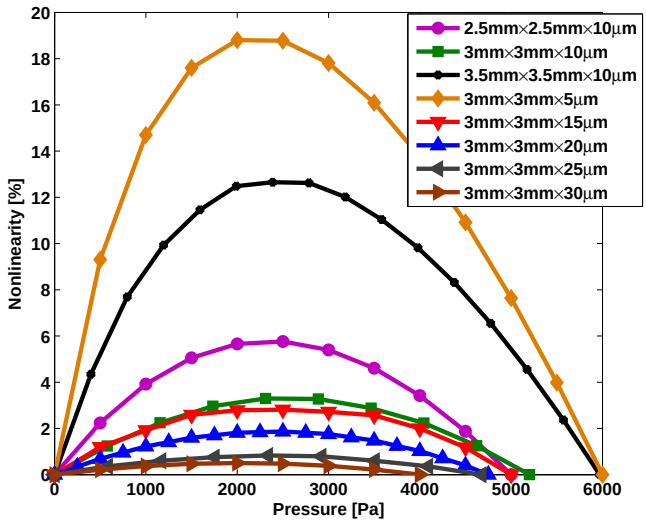

Figure 3.10: The nonlinearity between output voltage and pressure, when the glucose concentration is 150 mg/dL.

increased, it would lead to a decreased response time as per equation (3.15).

$$\frac{1}{t} = \frac{\frac{K_p}{\eta d_m} A(\sigma \Delta\pi - \Delta P)}{HA} \tag{3.15}$$

where t is the response time, H is the height of the device cavity and A is the area of the semi-permeable membrane. The response time is 60 min for the device having dimensions 3.5 mm $\times$ 3.5 mm $\times$ 10 μm which is high compared to 35 min for the case of device having dimensions 2.5 mm $\times$ 2.5 mm $\times$ 10 μm. Reducing the size of the cavity decreases the response time, however the sensitivity will be reduced. When the size is smaller, the filling of reference glucose solution inside the cavity and sealing with a semi-permeable membrane is a challenging job. Therefore the size of the cavity need to be carefully decided. The thickness of the Si membrane and the area of the semi-permeable membrane also affect the performance of the device. If the area increases, the volume flow increases and as a result response time will be decreased. This is because, the rate of displacement is more, and the steady state value is reached very quickly. The increase in area is not advisable because it brings nonlinearity to the system. The response time can be decreased by constraining the displacement of the Si membrane, that is, by increasing the thickness of the membrane. The disadvantage of increasing membrane thickness

is that the sensitivity will be reduced. The thickness of the membrane decides the amount of fluid that can pass through the semi-permeable membrane for a particular concentration difference. The design parameters of an osmotic pressure sensor is summarized in Table 3.3. Two different devices have been chosen with different Si membrane thicknesses of 10 μm and 25 μm, but having the same area of 3 mm $\times$ 3 mm.

Table 3.3: Design Parameters

Si membrane	Area Thickness Cavity depth	3 mm $\times$ 3mm 10 μm & 25 μm 475$\pm$2 μm
Semi-permeable membrane	Area Thickness MWCO	3 mm $\times$ 3mm 178 μm zero

3.5 Summary

The structural and electrical behaviors of an osmotic pressure sensor were studied using a commercially available FEM software tools. Three different types of pressure sensing techniques such as capacitive, piezoelectric and piezoresistance were analyzed. The piezoresistive pressure sensing technique has been chosen because of its linearity and simpler fabrication steps compared to other two techniques. The fluid flow through the semi-permeable membrane was analyzed using the FVM. The relation between the fluid structure interaction was studied by coupling three different equations (Navier-Strokes equation, ALE, and theory of elasticity). Finally, two different devices were chosen for the fabrication by considering the device parameters.

4

Fabrication and Packaging of an Osmotic Pressure Sensor

Contents

4.1 Introduction

In recent years, the advancement in the field of micro-machining technology has helped the batch fabrication of MEMS devices such as a microactuators, micro-cantilevers and pressure sensors for various kinds of applications. MEMS pressure sensors offer low cost and ease in fabrication, and the process steps are compatible with the CMOS fabrication. However, the challenging part is packaging of MEMS devices because most of them need to interact with the environment [53, 54] such as fluids, chemicals, gases, temperature, sound or mechanical excitations and moreover, the end results are measured in terms of voltage or displacement

or flow velocity or change in resonance frequency. Finally, the device need to be packaged to provide mechanical protection with provision for an interface between the MEMS device and the environment to produce the desired output. MEMS devices require application oriented packaging, and it is difficult to develop a standard method like in IC packaging [55]. The packaging of MEMS devices is challenging compared to conventional integrated circuit (IC) packaging, since many of the devices contain 3D movable structures which need to be protected, and simultaneously meet the basic demand that packaging should not affect the performance [56]. If the device experiences any stress during the packaging, it may lead to the deformation of the device since the MEMS device are very sensitive to external stress. Generally, the packaging cost can be upto to 80% of the total cost of a MEMS product because of its wide range of applications [53, 57].

The materials adopted for the MEMS packaging are ceramic, metal, epoxy, glass and plastic [58]. Indeed, cost-effective MEMS packaging methods are essential. Packaging of MEMS devices are classified into three groups: wafer level packages, plastic molded packages and cavity packages. In the case of wafer level packaging, device fabrication and packaging process are fully integrated. Traditionally, Si and glass materials are greatly used in the MEMS device fabrication and packaging because these materials show superior mechanical properties and are suitable for many applications [59]. The glass cavities are used as a cap to provide the mechanical protection and electrical isolation. And also the glass is used as a intermediate layer in wafer level packaging. The difference in the thermal expansion between Si and glass induces stress when they are bonded together. Plastic packaging like epoxy molding compound (EMC) mold technique is promising for the MEMS devices as a result of its low price and simple process. MEMS devices may be encapsulated by cap wafers before exploiting over-molding techniques, just like the conventional IC packaging. However, the EMC shrinks and generates stress, on the device during the curing process. MEMS devices are liable to external mechanical stress and can affect the performance of the device, which to a certain extent may be reduced by using EMC cavity packaging [53]. Cavity package consists of a substrate, a cavity wall, and lid on the top. The cavity packaging is more suitable for MEMS device and it will be shielded from the

external stress. Even though, ceramic and metal cavity packages provide great performance and reliability, and they are limited in application because of the material cost is comparatively high [58]. Packaging of Bio-MEMS affects the performance, because it involves high temperature processing while embedding the device and sealing with cavity [56]. Bio-MEMS, especially for those devices which interacts with fluids and other biological components, require alternative soft or polymeric materials such as silicone rubber, polycarbonate (PC), isobornyl acrylate, and poly-imide for the packaging [58, 60, 61]. Plastic cavities would be a great choice due to reasons such as their formation at lower cost and their transparent properties [58].

In this chapter, we have focused on the fabrication and packaging of an osmotic pressure sensor. The designed osmotic pressure sensor is fabricated by employing a bulk micro-machining technology on a SOI substrate. This allows for batch fabrication as well as the integration of electronic circuit on the same substrate. The device consists of a square cavity on the bottom side with a thin Si membrane on the top and it is constructed by etching the bulk Si using the DRIE Technique. The piezoresistors on the top side of a Si membrane are formed by boron diffusion. The final step is metallization using the thermal evaporation technique to provide the metal contacts for the piezoresistors. A routine I/V characterization has been carried out to check the resistance value of the piezoresistors and metal contacts. The fabricated device is packaged such that it can interact with liquids and gases. The device is packaged using the Polycarbonate (PC) material by employing a simpler technique instead of following the standard procedure for the packaging. Initially, the wafer is diced using the diamond cutter to separate the individual devices. The device is bonded to the fabricated PCB for the wire bonding. A PCB is attached into the PC flat sheet, and the electrical connections are isolated from interacting with fluids, and the mechanical protection is provided on the top with a cavity-cap. The advantages of the present technique are, the comparatively lower cost PC material and the flexibility it provides to house wafer level devices, especially the ones used for the biomedical devices like microactuators, glucose sensors and drug delivery pumps. The temperature required to complete the process is low and therefore thermally induced stress are be reduced to a certain extend. Moreover, we have not used any anodic bonding or lithography technique

in the suggested method. After packaging, the device performance is analyzed by applying external pressure using a commercial blood pressure monitor. The pressure applied is 0 to 30 mmHg and the corresponding voltage measured across the Wheatstone bridge circuit is 0 to 18 mV. The sections of this chapter are as follows. The fabrication and packaging of piezoresistive pressure sensor are presented in, section 4.2 and 4.3, respectively. The performance of the device is discussed in section 4.4 and finally the chapter is summarized.

4.2 Fabrication of a Piezoresistive Pressure Sensor

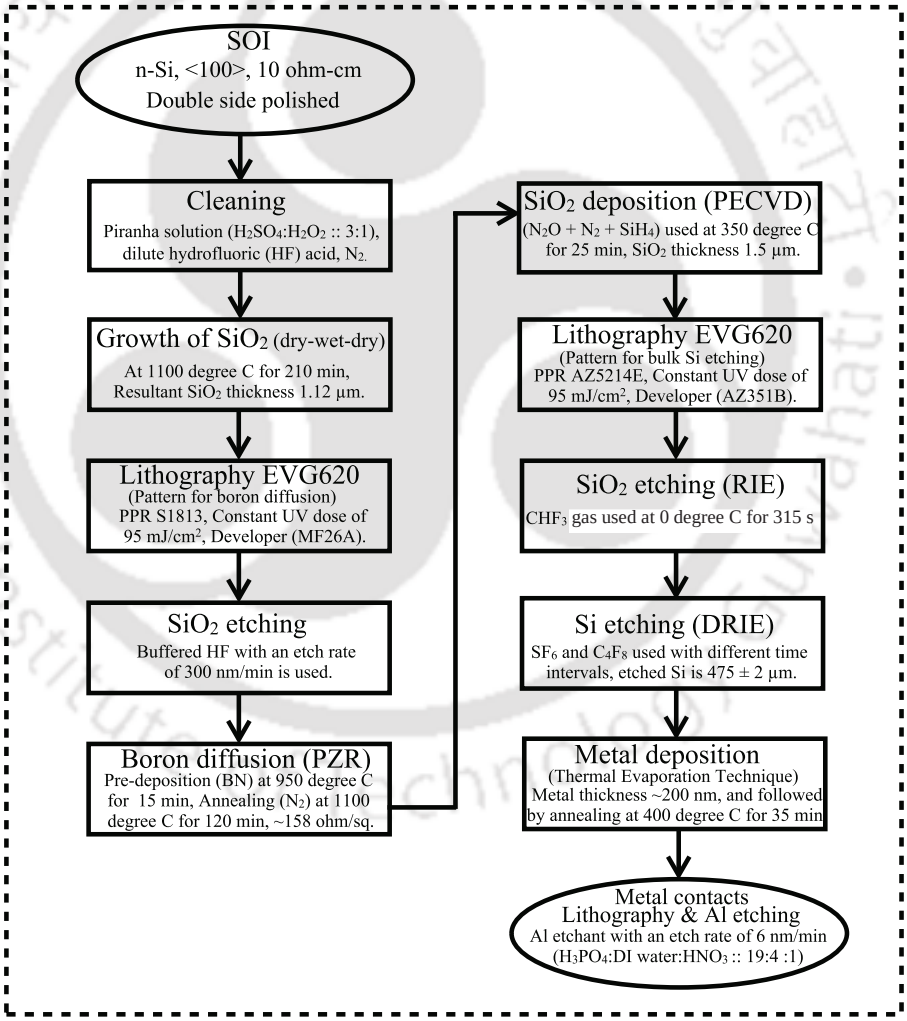

Figure 4.1: Process flow for the fabrication of piezoresistive pressure sensor.

The piezoresistive pressure sensor is fabricated on an N-type (100) double side polished SOI substrate. The masks for the piezoresistors, back side etching and contact pads are graphically

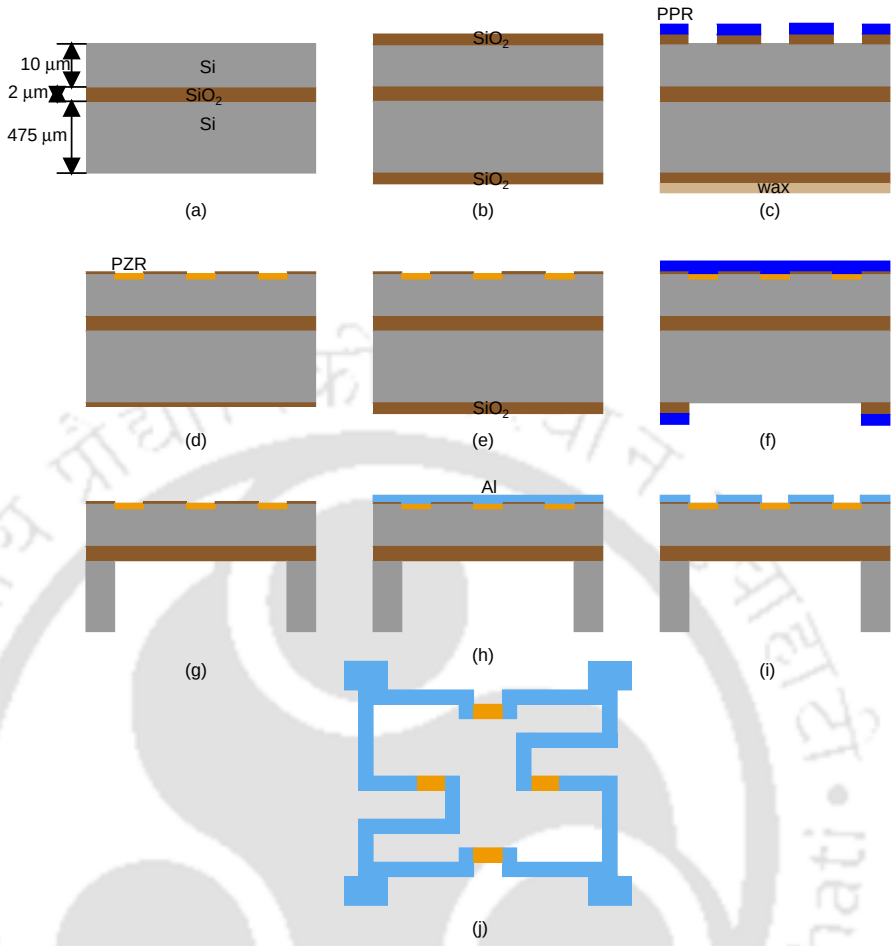

Figure 4.2: The cross sectional view of wafer after some of the major steps (a) Starting SOI wafer, (b) Growth of SiO_2 layer on Si, (c) Lithography and oxide etching to make windows for piezoresistors, (d) Boron diffusion, (e) SiO_2 deposition using PECVD, (f) Lithography and oxide etching to make a window for back side Si etching, (g) Bulk Si etching using DRIE, (h) Aluminium deposition, (i) Aluminium etching and (j) Top view of metal contacts.

designed and written using a Laser writer. Devices have been fabricated with different membrane thicknesses of 10 μm and 25 μm, and having the same area of 3 mm $\times$ 3 mm. Fig. 4.1 summarizes the process flow employed for the realization of the designed piezoresistive pressure sensor. Fig. 4.2 shows that the cross sectional view of the wafer, after some of the major steps involved in the fabrication. The starting substrate is an SOI wafer of a thickness of 485 $\pm$ 2 μm, approximately, and it includes a 10-μm silicon at the top and 2 μm SiO_2. The dimensions were verified using an optical profilometer. Initially, one can focus on the wafer top surface, and then, focus on background surface by changing the optical profilometry head in vertical (z)

direction. The difference in z value will give the wafer thickness. The wafer size was six inches, but it has been diced into smaller portions of 2–3 inches to make the devices.

Figure 4.3: The samples are dipped in piranha solution for cleaning.

The resulting cross sectional view of a single device is shown in Fig. 4.2(a). The wafers are cleaned using piranha solution (Fig. 4.3) and dipped in dilute hydrofluoric (HF) acid to remove any native oxide present. A thermal oxidation (dry-wet-dry oxidation sequence) step is carried out, at 1100 °C for 210 min, to grow a SiO_2 layer on the Si surface as shown in Fig. 4.2(b). The measured oxide thickness (by Ellipsometer) is 1.12 μm which is close to the targeted thickness of 1 μm. This oxide layer serves two purposes; first it provides an isolation between piezoresistors and secondly, its use as a mask for the subsequent boron diffusion process.

The wafer is subjected to the first lithography step, in order to transfer the patterns for boron diffusion. Prior to the photoresist coating the mask and the wafers are cleaned and dehydrated properly. S1813, a positive photoresist (PPR) is coated on the front side of the wafer over SiO_2 using a spin coater. The cross sectional view after spin coating is shown in Fig. 4.2(c). Speed of the spin coater is set to 4000 rpm and spinning is carried out for 45 s, in order to get the uniform thickness of 1.2 μm photoresist. The samples are prebaked at 95 °C for 1 min to harden the photoresist. Patterns are transferred onto the substrate after the exposure to a constant UV dose of 95 mJ/cm^2 using the EVG 620 mask aligner. The developed wafer is wet-etched with buffered HF (BHF) acid to remove any oxide present in the windows. The cross sectional view of the wafer after this step is shown in Fig. 4.2(c). The back side oxide

is covered with wax for additional protection. The oxide on the back side is not removed as it would act as a protection mask during the subsequent bulk Si etching. Fig. 4.2(c) shows that the oxide is etched only in the windows opened for boron diffusion. Complete removal of the oxide can be observed when the hydrophilic oxide is changed to a hydrophobic surface of the Si. The same was confirmed by a microscope also.

P-type Si single crystal piezoresistors are formed by boron diffusion step and the cross section is shown in Fig. 4.2(d). Boron diffusion is carried out in a thermal furnace using a ceramic source of boron nitride (BN) disk. Initially, a constant source diffusion is carried out at 950 °C for 15 min in the N_2 (2 liters/minute) ambient in order to place a known dose in a shallow layer on the surface of the Si. The BSG (borosilicate glass) deposited on the wafer during this constant-source diffusion is removed using a BHF solution. The sheet resistance measured after the pre-deposition is 98.51 Ω/m^2. The boron is diffused deeper into the Si wafer during a subsequent high-temperature limited-source diffusion (or drive-in) step. The oxide grown during the annealing is removed using a BHF solution. The sheet resistance measured after the drive-in is 158 Ω/m^2. During the etching of the BSG, the thermally grown oxide on the back side, has been thinned down and the cross-sectional view is shown in Fig. 4.2(d). In order to etch the bulk of Si using a standard process like DRIE, the oxide mask need to be thicker. The SiO_2 layer is deposited on the back side using a Plasma Enhanced Chemical Vapor Deposition (PECVD) step and the cross-sectional view is shown in Fig. 4.2(e). The total oxide thickness measured (by Ellipsometer) is 1.5 μm.

A second lithography step is employed to transfer the patterns to the back side of substrate, to define the windows for etching of bulk Si. Using a double side alignment technique, Mask-2 is aligned to the top side of wafer corresponding to the alignment marks formed during the previous boron diffusion, and the wafer is exposed to UV for 5 s. The oxide is etched from the opened windows using the reactive ion etching (RIE) step. The resultant cross-section is show in Fig. 4.2(f). The DRIE is used to etch the bulk Si from the back side, to form a square cavity reaching till the oxide layer. The Si is etched with two different recipes; the etch rate for the recipe one is 28-29 μm/min and it is carried out for 15 min. The recipe two is 2-3 μm/min and

it is carried for 10 min. The Si etching is stopped exactly at the buried oxide layer as shown in Fig. 4.2(g).

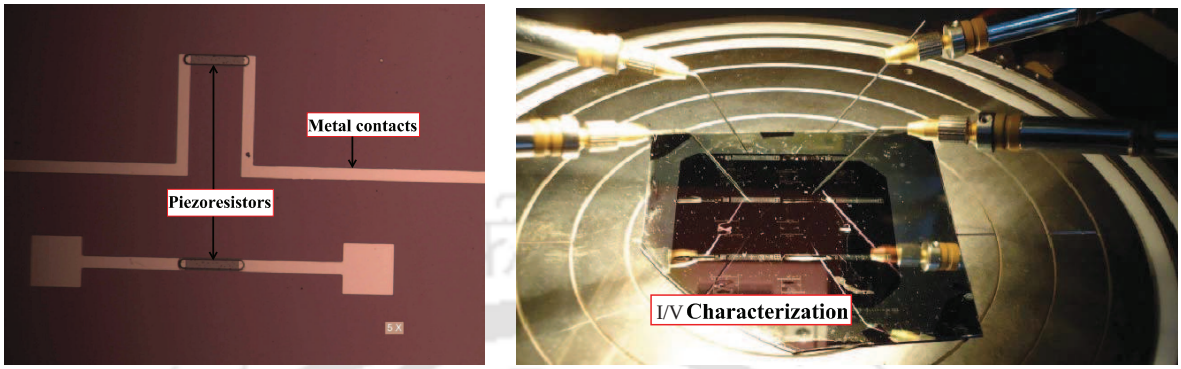

(a) (b)

Figure 4.4: (a) Metal contacts for the piezoresistors (b) and I/V characterization using DC probe-station.

The next step is a metallization, to provide the metal contacts for the piezoresistors. A 200 nm thick aluminum is deposited on the top of wafer by thermal evaporation process and resultant cross-section is shown in Fig. 4.2(h). After the deposition of aluminum, the wafers are annealed in forming gas in order to reduce the resistance of the metal contacts. This reduction is due to the expansion of crystal grain boundaries. Third lithography step is employed to transfer the patterns for the metal contacts. Before coating the photoresist on the top side of the substrate, the wafers are mounted on a dummy wafer, to avoid any breakage of the very thin diaphragm formed after the bulk Si etching. The wafers are exposed to UV at a constant dose of 95 mJ/cm^2 and are developed to remove the photoresist from the exposed areas. The step is shown in Fig. 4.2(i). Aluminum etching is carried out at room temperature with an etchant (wet etching) and the metal contacts connected to the piezoresistors can be seen in Fig. 4.2(j) and Fig. 4.4(a). After the device fabrication, the I/V characterization is carried out using DC probe-station (Agilent 4155C) to check the metal contacts and resistance values of the piezoresistors as shown in Fig. 4.4(b). The measured resistance value is 160±3 Ω/sq approximately. The input voltage is varied from 1 V to 5 V and the corresponding current is observed. The V/I ratio is found to be constant for most of the devices, for different input voltages.

4.3 Packaging of a Piezoresistive Pressure Sensor

The package, involves several processing steps, beginning with the dicing of device and concludes with the sealing of device for the mechanical protection, each stage is monitored to meet the desired performance. Fig. 4.5 summarizes the process flow developed for the packaging of the fabricated piezoresistive pressure sensor. The wafer contains 9 devices with appropriate spacing for the dicing as shown in Fig. 4.5(a). The wafer is diced using the diamond cutter to separate the individual devices. A single device is shown in Fig. 4.5(b). After dicing, a PCB is designed and fabricated according to the patterns of metal bond pads of the device and their dimensions. The fabricated PCB contains metal bond pads made up of gold and a square shaped window is provided in the center for the device housing. The device is bonded to the PCB using a die bonding epoxy adhesive and the curing temperature is set at 150° C for 60 min. The top view of device after this step is shown in Fig. 4.6.

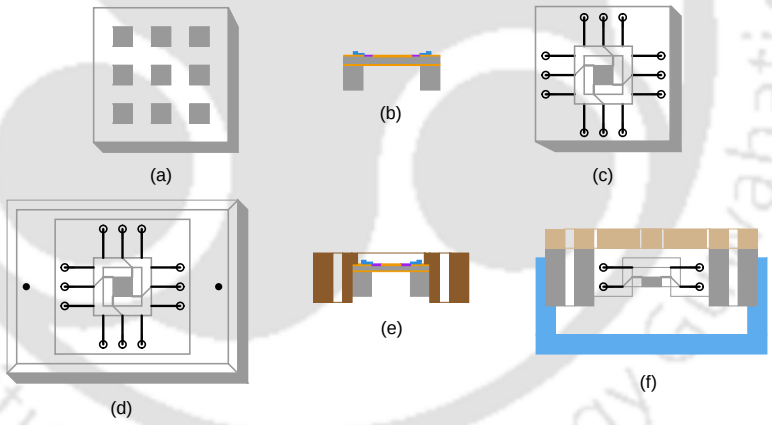

Figure 4.5: Process flow for the packaging of piezoresistive pressure sensor (a) Device fabrication, (b) Wafer diced using a diamond cutter, (c) Device embedded in a PCB, (d) PCB mounted on a PC flat sheet, (e) Cross sectional view, (f) Top side sealed with PC cavity cap.

The electrical contact between the metal bond pad of the device and the pad on the PCB is made by wire bonding. Wire bonding is an important process and the device performance might get affected if the bonding strength is weak. Both PCB and device are cleaned prior to the wire bonding to remove any dust particles and organic components present so that the bonding strength is improved. The wire bonding is carried out using the wedge bonding technique and the wire employed is of aluminium metal having a diameter 25 μm. After the wire bonding,

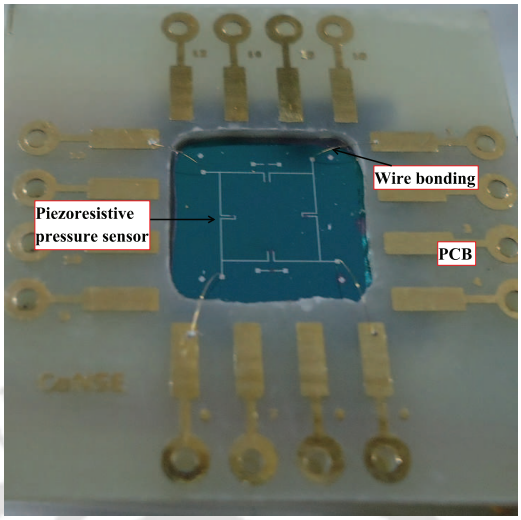

Figure 4.6: The device is bonded into a PCB.

the device packaging is initiated. Polycarbonate material is chosen as the packaging material and it has the excellent mechanical properties compared to other polymeric materials and it is transparent in nature. The Young's modulus and tensile strength of PC are 2.3-3 GPa and 60-70 MPa respectively [62]. PC is a soft and flexible material with processing temperature in the range of 280-330° C. PC material is cheap and it is available as flat sheet with different sizes in different thickness. However, the weakness of the PC is that it reacts with certain chemicals such as solvents, aromatic hydrocarbons, esters, and ketones. Indeed, the traditional wafer cleaning process is not feasible for PC, such that when it reacts with acetone, methanol or isopropanol, a streaked white discoloration is observed. Therefore, PC is cleaned only with water and then properly dehydrated.

The PC flat sheet is diced into the rectangular plates according to the desired dimensions. The square window is opened in the middle of the rectangular plate using a Lathe machine. This is to provide the housing for the PCB including the device. The PCB is mounted in a PC flat sheet, and the device cavity on the bottom side is kept open such that it can interact with the environment (osmotic liquids, gases, and external pressure) as shown in Fig. 4.7(a) and Fig. 4.7(b). The M-Bond 200 adhesive is used to provide the bonding between PCB and PC flat sheet. This process is carried out at the room temperature and it is very easy to handle,

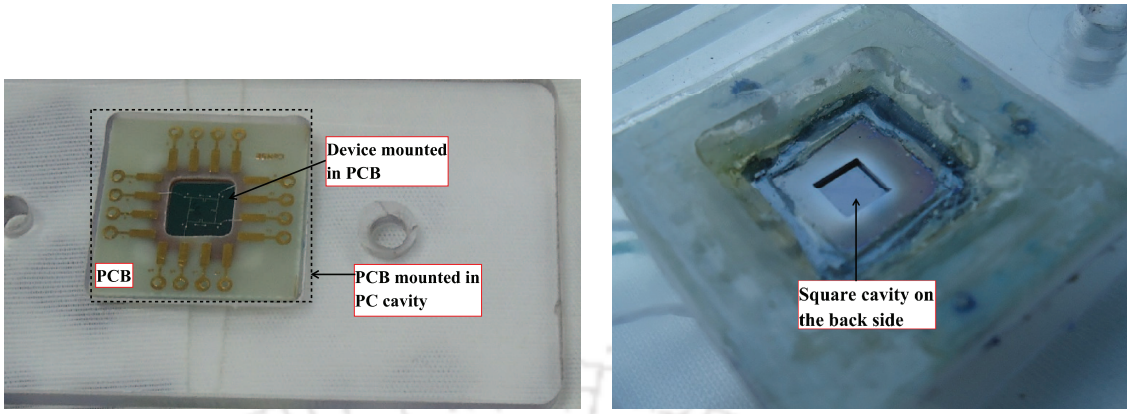

(a) (b)

Figure 4.7: (a) The device is mounted into a PC square cavity (b) and the square cavity of the device kept open to interact with environment.

and cures almost instantly to produce an essentially creep-free, fatigue-resistant bond. Finally, the top side is sealed with the square cavity cap made up PC flat sheet to provide mechanical protection as well as the isolation for electrical contacts from fluids. Depending on the application, the top side square cavity cap can be sealed permanently, or else a locking system is provided between the top and the bottom plate. The provision is made for the packaged device to interact with osmotically active liquids so that any change in osmotic pressure can be monitored.

4.3.1 Fabrication of a Testing Chamber

The test chamber is designed and fabricated according to the dimensions of the packaged device. The test chamber is fabricated using the polymethyl methacrylate (PMMA) glass. The acrylic sheet thickness is 5 mm, diced into rectangular plates using the Lathe machine and bonded with chloroform to make the rectangular cavity as shown in Fig. 4.8(a). The rectangular cavity is filled with the solution under test. The inner dimensions of the testing chamber are 80 mm length, 40 mm width, and the depth 20 mm. Provisions are made for inlet, outlet and for placing piezoresitive pressure transducer on the top side of the testing chamber. The packaged device can be fixed exactly into the test chamber so that it can interact with fluids. Eventhough, this device is packaged for fluidic application, it can be used for other

purposes such as measurement of external pressure, temperature and gases. The packaged device is attached to the fluidic test chamber, to test the device for the fluidic applications as show in Fig. 4.8(b).

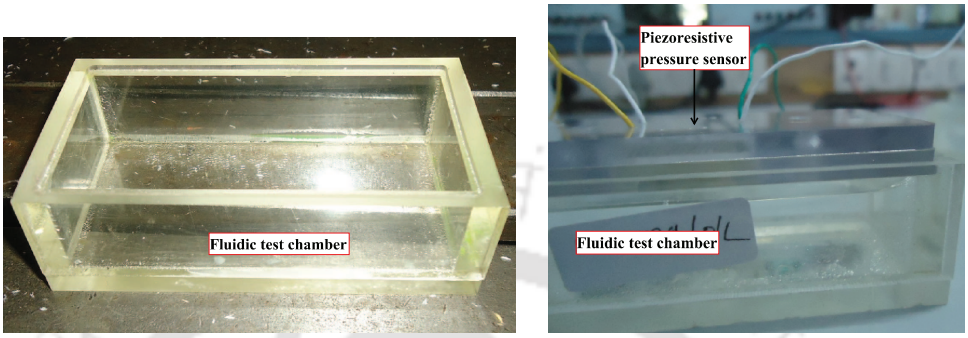

(a) (b)

Figure 4.8: (a) Testing chamber with a rectangular cavity to fill the fluid (b) and the packaged device is attached to the fluidic testing chamber.

4.4 Performance Testing

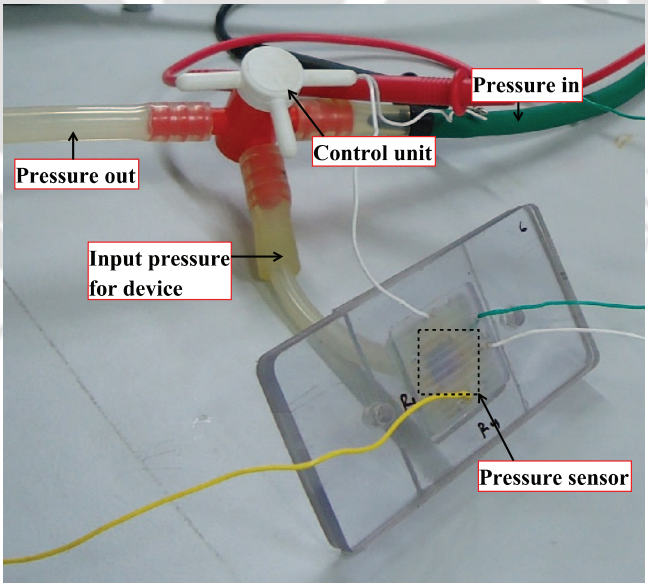

Figure 4.9: Packaging of a piezoresistive pressure sensor.

After packaging, the performance of the device is tested by applying an external pressure. Fig. 4.9 shows the setup used to measure the performance of the piezoresistive pressure sensor. During the packaging a provision was provided to facilitate the application of external pressure

on the bottom side of the device. A small hole is made in the squared acrylic sheet, and it is exactly matched to the cavity of the device on the bottom side. The squared acrylic sheet is bonded to the packaging device using an instant adhesive material (Araldite Klear). A plastic tube is fixed into the hole with the same adhesive material as passage for the external pressure. The plastic tube has provision for a coupler by which the flow can be tuned on or off and it is connected between blood pressure monitor and device as shown in Fig.4.9. The device is tested by applying external pressure and its value is monitored using a commercial pressure gauge which is already calibrated. The pressure applied is from 0 to 30 mmHg and the corresponding voltage across the Wheatstone bridge configuration is 0 to 18 mV as shown in Fig.4.10. The sensitivity of the pressure sensor is 0.120 mV/mmHg/V. The above data confirms that the device is suitable for low pressure sensing applications. For the glucose sensing application one is typically looking for a resolution of a 20 mg/dl which corresponds to 1.5 kPa for the pressure sensor in this work.

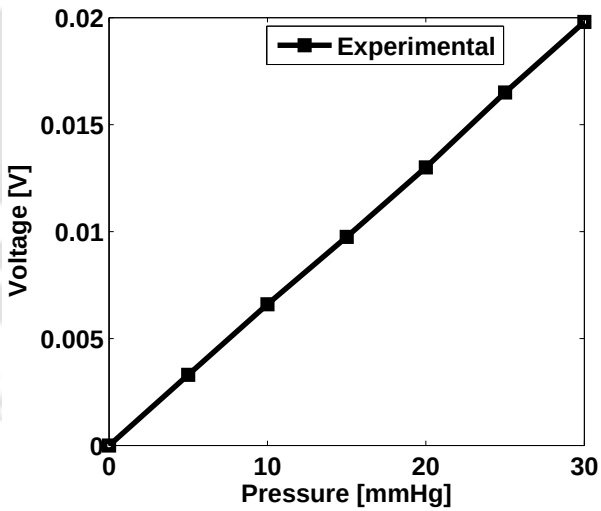

Figure 4.10: The output voltage observed across the Wheatstone bridge for the external pressure.

4.5 Summary

The piezoresistive pressure sensor was fabricated and it was packaged in a cavity made on PC material by employing a simple technique. The packaging cost was low because of

the PC material and it does not need steps like a lithography, etching, or anodic bonding. The temperature employed to house the device in the cavity on PC material was low there by thermally induced stress was reduced. The voltage across the Wheatstone bridge was measured by applying known values of pressure externally. The sensitivity of the sensor can be affected by temperature variations. Further, the temperature effect on the packaged device was negligible, and the device performance was tested by varying the temperature from 24-36° C. For a 24-36° C change in the temperature, less than 2% change in output voltage was observed and this change was not very significant for the present application. The PC material provides excellent mechanical properties and transparent in nature unlike the other polymers. Moreover, the PC was a soft and flexible material, and it was a great choice for the packaging of actuators, pressure sensors and the fluidic interaction devices. The PC seems to be a promising material for the packaging of prototype devices and it dose not require any specific equipment. In a laboratory setting, a manual operation would be enough to package the device with low cost.

5

Experimental Setup and Testing of an Osmotic Pressure Sensor

Contents

5.1 Introduction

MEMS devices are increasingly becoming popular owing to their wide applications. The pressure sensors are integral part of many systems like sensing, diagnostic, glucose monitoring or drug delivery. MEMS devices are integrated with fluidic devices or interacted with fluids for specific applications of glucose sensing and insulin delivery. Chemical-free osmotic pressure sensors are prominent for the glucose sensing application as these employ simple sensing technique. In 1996, Nagakura et al. [17] fabricated a chemical-free, autoregulated osmotic pump for insulin delivery. An osmotic pump can delivery the insulin according to the change in glucose concentration levels; however, their size is large (21 mm × 20 mm), and it is made from a poly-

mer material. The osmosis principle is further exploited to develop an implantable devices [16]. Another implantable sensor, based on the volume change due to the flow of water across the semi-permeable membrane, has been developed [18] to monitor osmotically active components, such as glucose. It is capable of continuous glucose monitoring since the system is employed with a feedback loop, but the system is large and has a longer response time. Although the operation of these devices is free from chemical reactions, they suffer from having lower sensitivity, longer response time and larger size. Hydrogels which have glucose affinity are employed to improve the sensitivity and selectivity. The hydrogel is confined inside a pressure sensor to facilitate the measurement of change in glucose concentration levels [21, 22, 23]. However, the response time of theses devices are long.

In this chapter, we have demonstrated an osmotic pressure sensor, that utilizes the osmosis principle to measure the glucose concentration levels. The geometrical parameters of the system plays a major role and they determine the response time, sensitivity and linearity of devices, and therefore efforts have been taken, to reduce the dimension of the presented system. By considering these effects, two sets of devices having membrane thickness of 10 μm and 25 μm are tested and their results are compared with respect to each other. The osmotic pressure sensor is successfully demonstrated for the measurement of different glucose concentration levels ranging from 50 mg/dL to 450 mg/dL. Further, the simulation results are validated with the experimental results. This chapter is further organized as follows. The section 5.2 experimental setup. The results and discussions are presented in section 5.3 and finally, the chapter is summarized.

5.2 Experimental Setup for an Osmotic Pressure Sensor

Fig. 5.1 shows the schematic diagram of the glucose sensor. The packaged pressure sensor is attached to a fluidic test chamber, and its size is very large compared to the device. The fluidic test chamber volume is kept around 64 mL compared to the device volume of 4.275 μL, in order to maintain the glucose concentration in the test chamber constant during the process. The pressure sensor has a square cavity, which is constructed on an SOI substrate by using

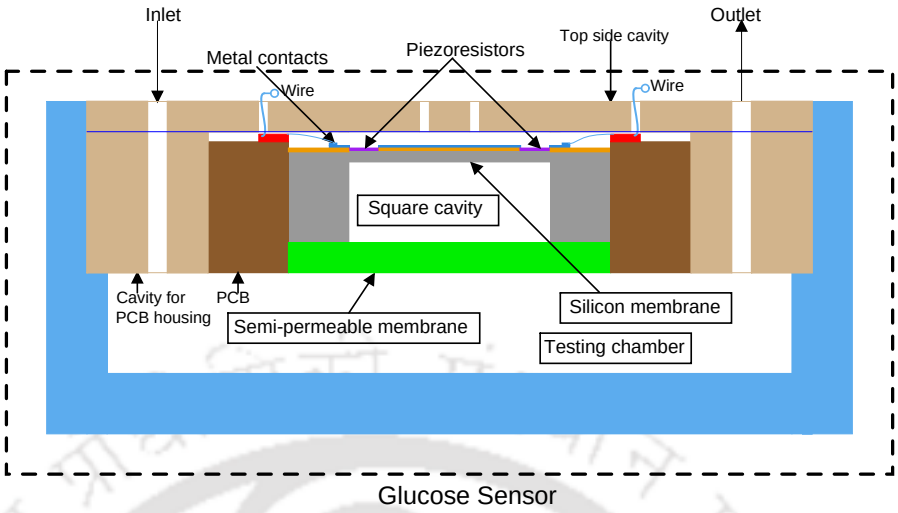

Figure 5.1: Glucose sensor based on osmosis principle. Inside the square cavity a reference glucose solution of 100 mg/dL is placed. Inside the test chamber the glucose solution is varied from 50 mg/dL to 450 mg/dL.

bulk Si micro-machining technology. Moreover, Si has excellent mechanical properties, which are required for reproducible elastic deformations under identical loads [51]. DRIE technique is used to etch the bulk Si from the back side to form a square cavity with a depth of 475 $\pm$ 2 μm. Two devices are chosen with different diaphragm thickness of 10 μm and 25 μm, but having the same area of 3 mm $\times$ 3 mm. The square cavity is filled with a standard glucose solution at a reference concentration. A Si membrane is constructed on the top side, and a semi-permeable membrane is used to seal the filled cavity on the bottom side. When the device is exposed to glucose solution in the fluidic test chamber, due to osmosis, the solvent (water) diffuses into the higher concentration side if there is a concentration difference across the semi-permeable membrane. The in/out flow of solvent through the semi-permeable membrane introduces the volume change inside the cavity, which causes a displacement in thin Si membrane (thickness of 10 μm and 25 μm), compared to the firm semipermeable membrane (thickness of 178 μm).

5.2.1 Experimental Setup

The test setup as shown in Fig. 5.2, is prepared for the glucose sensor to measure any change in glucose concentration levels. The square cavity on the bottom side of the glucose sensor is cleaned using acetone and is followed by isopropyl alcohol (IPA) to remove any dust

particles. White crystal powder of d-glucose ($C_6H_{12}O_6$) is used to prepare glucose solutions by adding the required amount of high purity deionized (DI) water. A glucose concentration of 100 mg/dL is prepared by adding 100 mg of d-glucose in 100 mL of DI water. A series of glucose solutions are prepared, having concentrations ranging from 50 mg/dL to 450 mg/dL, by adding suitable amounts of d-glucose (*i.e.*, 50 to 450 mg) into 100 mL of DI water.

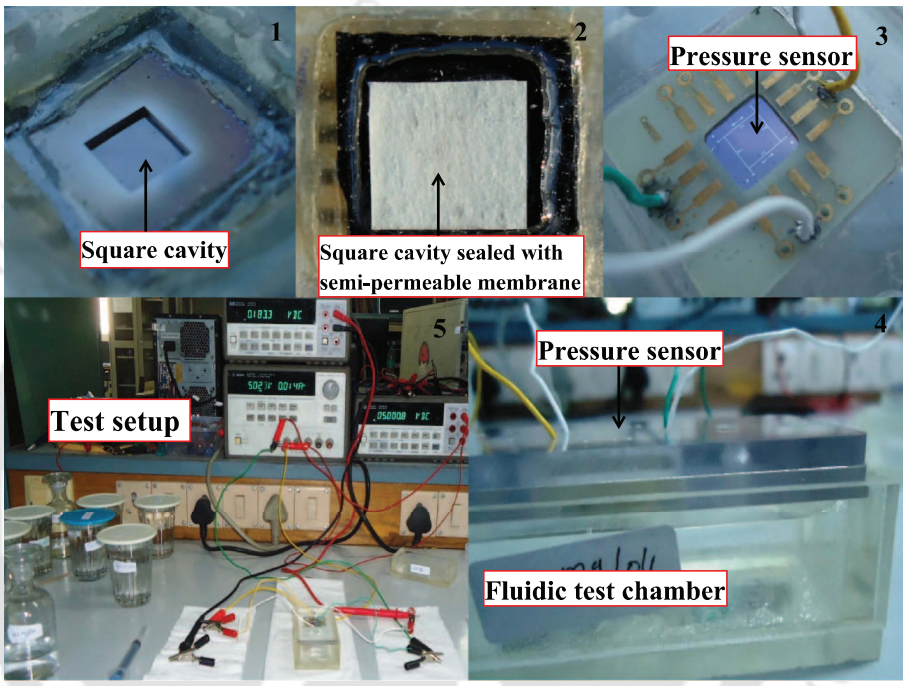

Figure 5.2: Glucose sensor with a testing chamber attached on the bottom side.

Before the device cavity is filed with any solution the output voltage across the Wheatstone bridge is measured to determine the offset voltage; it is approximately 1 mV. To begin the testing, the square cavity is filled with a standard glucose concentration of 100 mg/dL. We use an Accupipet (500 nl resolution) to fill the square cavity. An Accupipet of 0.5 μl resolution is used to fill the square cavity. The cavity was filled very slowly in multiple steps with controlled amount to avoid any air-bubbles. Even if some air-bubbles are trapped during the bonding time, it will not be the problem because they can pass through the porous medium. Please note that the device is not attached to the test chamber at this time. The filled square cavity is sealed manually with a semi-permeable membrane. A cyanoacrylate based adhesive material is used for attaching the semi-permeable membrane to the silicon. The glue swells in the presence

of water due to rapid polymerization, forming long, strong chains, joining the bonded surfaces together. Many trials are carried out on dummy samples by applying the glue fist and then filling the solution. After many trials, it is found that it is better to fill the solution first and then apply the glue, finally putting the semi-permeable membrane into place. A very sharp needle is employed to apply the right amount of glue; this is done carefully under a magnifying glass, not very close to the edge of the cavity. In this way any chemical interference between the glue and the glucose solution is avoided, but at the same time the glue should be spread close to the edge of the cavity while the pressure is applied for bonding. Once the glue is dry it is found that it will no longer react with the glucose solution.

Device is sealed with semi-permeable membrane. The semi-permeable membrane (YM-CESP3001, Sterlitech Corporation, Kent USA) employed is of a cellulose acetate material having properties, such as 97% of NaCl rejection and a pH range of 2–8. The molecular weight cut off (MWCO) of the membrane is zero. The MWCO defines the smallest solute that will pass through a membrane, and larger particles above the MWCO are rejected. The molecular weight of NaCl and glucose are 58.44 g/mol and 180.16 g/mol, respectively, and these molecules may not pass through the membrane. In comparison to these the molecular weight of water is 18 g/mol. The thickness and Young's modulus of the membrane are 178 μm and 12.781$\pm$2 GPa, respectively. The empty porous portions of the membrane is filled with solvent once the semi-permeable membrane comes into contact with the filled cavity, and subsequently, the membrane becomes wet. Though, we have introduced a 100 mg/dL solution to the chamber, some solvent is already absorbed by the membrane; therefore, the volume inside the cavity is decreased, and its glucose concentration is also increased. This causes a displacement in the membrane towards the cavity, and the output voltage is increased to 19.2 mV. Then, the device is attached with fluidic test chamber, as shown in Fig. 5.2. To characterize the device response time, the glucose concentration in the square cavity needs to be reset to the reference value of 100 mg/dL, *i.e.*, the output voltage needs to be brought back to the reference value close to zero. For this purpose, a glucose solution of 100 mg/dL is introduced into the test chamber, where it is allowed to permeate through the semi-permeable membrane, to interact with the

standard glucose solution in the device. The solvent moves from the test chamber into the device cavity, in order to balance the osmotic pressure. The voltage is decreased from 19.2 mV to 1.1 mV within 25 min. It has been observed that for the next 20 min, the variation in the output voltage is negligibly small and reached the reference point (close to zero) after 45 min, as shown in Fig. 5.3. In a separate measurement, a glucose concentration of 100 mg/dL is placed in the test chamber for 720 min, and the output voltage obtained was constant for the entire duration.

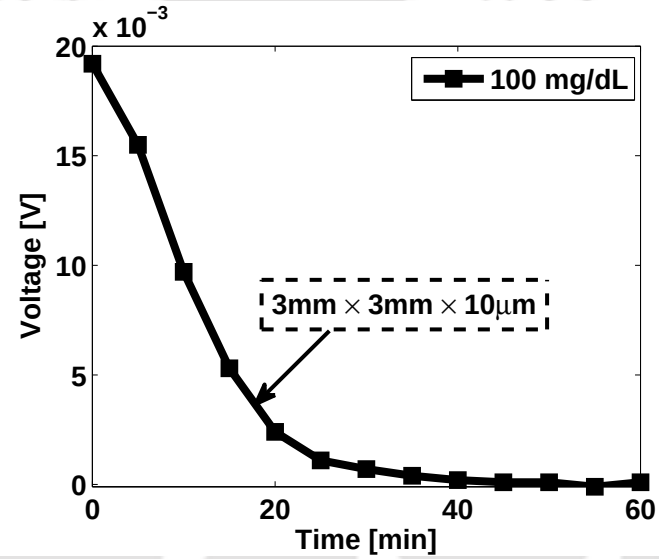

Figure 5.3: The output voltage is decreased when the 100 mg/dL glucose concentration introduced in the test chamber.

5.3 Results and Discussion

In this section, performance of the fabricated device is demonstrated successfully. The simulation results of designed osmotic pressure sensor is compared with experimental results, and followed by a comparison to other reported glucose sensors. After stabilizing the glucose solution inside the device to a reference value of 100 mg/dL i.e the output voltage is close to zero, then the 100 mg/dL in the fluid test chamber is replaced with 150 mg/dL, so that the concentration difference across the semi-permeable membrane is 50 mg/dL and a corresponding $\Delta\pi$ is developed as per equation (3.2). This causes a net flow of solvent from the sensor cavity,

which contains a lower concentration (hypotonic solution), into the test chamber having a higher concentration (hypertonic solution). The volume inside the cavity decreases as the solvent pass through the semi-permeable membrane into the test chamber, and it causes a displacement in the Si membrane.

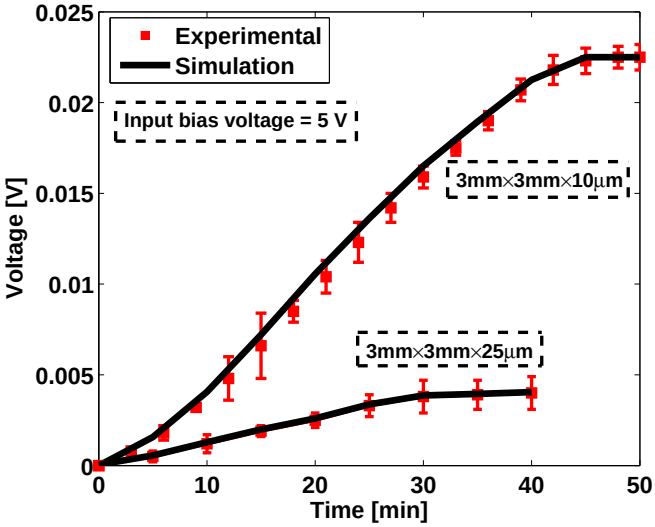

Figure 5.4: The response of a sensor for the glucose solution of 150 mg/dL when the concentration inside the cavity is 100 mg/dL.

Fig. 5.4 shows the change in output voltage corresponding to glucose concentration of 150 mg/dL outside the device. It is observed that the output voltage is increases linearly for a certain period of time and it finally reaches a steady state value. The output voltage reaches its maximum value of 21.6 mV after 40 min in the case of a device having the diaphragm thickness of 10 μm. This voltage was higher compared to the case where the diaphragm thickness was of 25 μm where, after 30 min it reached a maximum value of 3.8 mV as shown in Fig. 5.4. Eventhough, the operation continues further, the change in output voltage obtained is negligible. Further, the simulation results are closely matched with experimental results in case of 25 μm device. We have observed a slight deviation between simulation and experimental results for the 10 μm device and the error is about 10 %. The response time of an osmotic pressure sensor is characterized as the time required to reach a 95% of the steady state value of the output voltage for the change in glucose concentration in the test chamber (for example 150

mg/dL) [10]. The sensitivity of the glucose sensor is desired output (voltage in this case) per mg/dL of glucose concentration with respect to specific time and input source. The sensitivity (output voltage per [mg/dL] per voltage per time) for the 25 μm device is approximately 0.5 μV/(V·mg/dL·min) and it is low compared to 10 μm device which is 2 μV/(V·mg/dL·min), without any amplification of the output voltage. The sensitivity is high for smaller membrane thickness, as expected, but at the cost of increasing response time and nonlinearity.

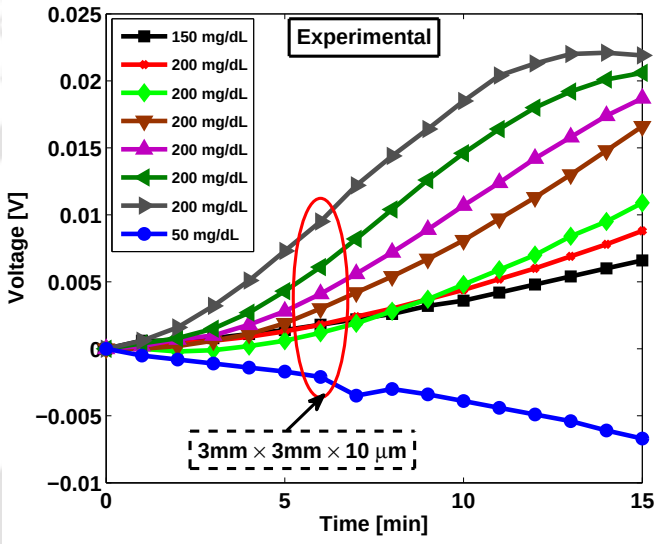

Figure 5.5: The output voltage as function of time, for different glucose concentrations in the test chamber.

The glucose sensor is tested with different glucose concentrations, ranging from 50 mg/dL to 450 mg/dL. Fig. 5.5 shows the output voltage of the glucose sensor for the different glucose concentrations. If Fig. 5.5 is extended till the settling time, the plots will be too crowded, and hence, a format, like in Fig. 5.6, is opted for, for better visibility. In each case, the concentration inside the cavity is reset to 100 mg/dL prior to the measurement of a new glucose solution in the test chamber. The time needed to reach the maximum value of the output voltage is different for each concentration, and it is shortest for the case where the test chamber contains the highest concentration of glucose, as shown in Fig. 5.6. The difference in glucose concentration across the the semi-permeable membrane with respect to the reference point of 100 mg/dL is shown on the x-axis. For instance, when the glucose solution in the test chamber is 450 mg/dL,

the output voltage attains its steady-state value within 15 min, as shown in Fig. 5.5. When the concentration is increased from 50 mg/dL to 450 mg/dL, the output voltage across the Wheatstone bridge is increased from -6.7 mV to 22.7 mV for the 10 μm device and it is from -1.7 mV to 4 mV for the 25 μm device as shown in Fig. 5.7.

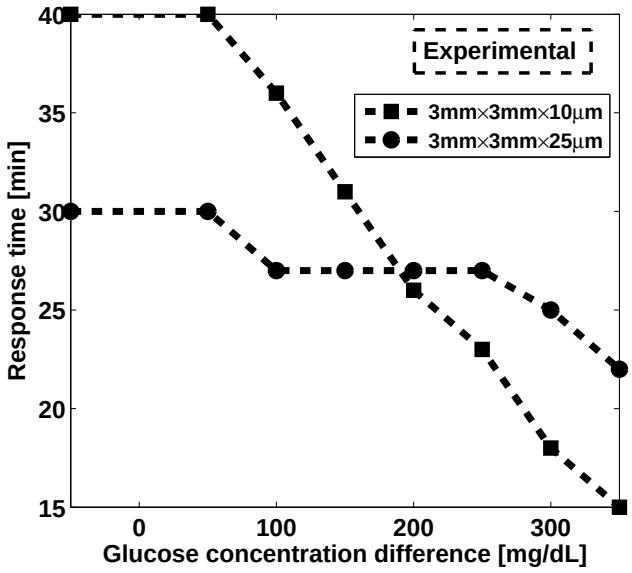

Figure 5.6: Response time of the osmotic pressure sensor for the concentration difference across the semi-permeable membrane.

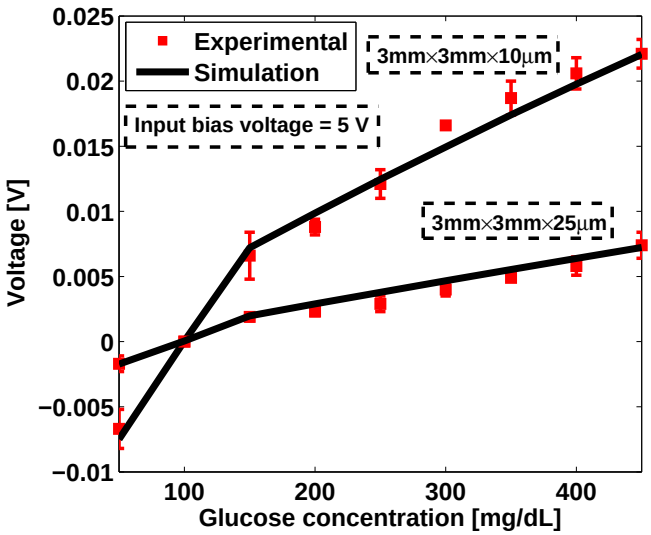

Figure 5.7: The output voltages obtained after 15 min of osmosis for different glucose concentrations.

The output voltage indicated in each case is the value obtained after 15 min of osmosis.

Fig. 5.7 summarizes the device behavior and provides a quantitative measure of the glucose concentration in terms of voltage. The simulation results and the experimentally obtained values are in close agreement for the 25 μm device, as shown in Fig. 5.7. However, a slight deviation is observed between simulation and experimental results for the 10 μm device and the error is about 10 %. The sensitivity obtained is in the range of 1 to 2 μV/(V·mg/dL·min) for the 10 μm device which is high compared to 25 μm device and it is from 0.3 μV to 0.5 μV/(V·mg/dL·min), without amplification of the output voltage, for the corresponding glucose concentrations ranging from 50-450 mg/dL. The variation in the output voltage is always found to be proportional to the glucose concentration change. The error bars indicate the variation observed during three consecutive measurements. The device is tested continuously for 8 days with different concentrations to verify the endurance of the device. The variation in the output voltage is always found to be proportional to the glucose concentration change. All the above measurements are carried out in room temperature ambient (26 °C to 28 °C).

The percentage of error between simulation and experimental results ere 10 %. In the simulation study $\Delta\pi = \Delta P$, when $\Delta w/\Delta t = 0$. However, in practical situations, ΔP will not reach to 6.9 kPa. This is because, as the Si membrane is being stretched, it brings increased resistance to the fluid flow. Finally, it reaches the steady state and prevents further solvent flow. The diffusion flow rate across the semi-permeable membrane is linear when the Si membrane effect is not considered. However, in practical scenario, the Si membrane opposes the further flow as the time progress because ΔP (the hydrostatic pressure when the effect of Si membrane is considered) is not enough to push the membrane any further and the steady state condition is already reached. Another reason might be the difference in deployment conditions.

The fabricated glucose sensor is able to measure a small variation (results for 50 mg/dL are plotted, but it could be as low as 20 mg/dL) in the glucose concentration levels. The performance comparison of the fabricated glucose sensors are presented in Table 5.1. The response time of the present glucose sensor is 30 min, which is lower compared to other reported works in [17, 21]. In the present work, the ratio of fluid volume change inside the cavity to the total volume of the cavity is high compared to the sensor in [17], and therefore, the response

Table 5.1: Performance comparison of fabricated glucose sensors.

Reference	Basic principle/Sensing mechanism	Selectivity	Any mechanical excitations involved?	Measurement quantity and instruments	Response time (min)	Device dimensions (μm)
[10]	Association/ dissociation (Viscosity change)	Yes	Magnetic excitation	Deflection is converted to voltage (Optical lever system and photodetector)	3	$\sim$(600 × 600 × 800) Rectangular cuboid
[11]	Association/ dissociation (Viscosity change)	Yes	Magnetic excitation	Capacitance is converted to voltage (Built-in capacitor)	1.5	500 × $\sim$500 × $\sim$530) Rectangular cuboid
[12]	O_2 consumption and production H_2O_2 (Surface stress change)	Yes	No	Deflection (Atomic force microscope and position sensitive detector)	$\sim$40	350 × 35 × 1) Cantilever
[17]	Osmosis (Volume change)	No	No	Displacement (Laser displacement meter)	120	21000 × 20000 Cylindrical
[21]	Association/ dissociation (Pressure change)	Yes	No	Pressure (Piezoresistive pressure transducer)	60±15	3180 × $\sim$420 Cylindrical
[Present work]	Osmosis (Volume change)	No	No	Voltage (Built-in Wheatstone bridge)	30 & 40	3000 × 3000 × 650 Square cuboid

time is shorter. Nevertheless, the response time of the present work is much higher when compared to a value of 1.5 min reported in [10, 11]. The response time is much smaller in those glucose affinity sensors [10, 11, 63], because the time needed for the glucose molecule to associate/dissociate with the polymer is smaller. The response time is high for the glucose sensor in [21], even though it involves chemical binding, due to the expansion or contraction time required for the hydrogel. In the case of the glucose affinity smart hydrogel, glucose solute molecules permeate through membrane [10, 11, 21], where in the present work, the solvent molecules flow through the semi-permeable membrane. Moreover, the present work is related to the volume change inside the cavity with respect to the change in glucose concentrations, which finally brings a deflection in the Si membrane, and like in [10, 11, 12, 21, 63], neither any chemical reactions nor any mechanical excitations are involved, so that the lifetime of the device is improved. The sensing mechanism employed in the present work is very simple compared to the other glucose sensing devices, as the variations in the glucose concentration levels are directly measured in terms of voltage, with the help of a simple Wheatstone bridge and a battery. In the case of the capacitance change reported in [11, 63], an external circuit is employed to convert the changes into a voltage. Another sensing mechanism is optical in nature, and the one required to detect the deflection in the cantilever beam corresponds to glucose concentrations [12]; such a method is not suitable for implantation purposes, and it is unstable in a mobile environment. Further, the present work requires very simple fabrication steps, and it is smaller in size compared to the sensor in [17]. The device lifetime of the present sensor is expected to be longer, since there are no chemical reactions involved.

The device might respond not only to glucose, but to similar substances, like de-hydration, ethanol, lactic-acid, amino acids, ascorbic acid and mannose [64, 22], if there is a substantial change in their concentration levels, and this will cause interference. Normally, the lactic-acid concentration levels are small, but during exercise, these will rise to higher levels. The ethanol and amino acids concentration levels are related to dietary aspects, and they can be maintained in a normal range, though they cannot be controlled at a constant level. The interference from other substances needs to be addressed for the improvement of this sensor. The selectivity of this

sensor may be improved by employing glucose affinity materials, like hydrogel or Concanavalin A-dextran [21, 22, 23], in the device instead of a standard solution. The sensing material employed in [22, 23] consists of Con A, which possesses an affinity toward glucose, and the equilibrium is perturbed by glucose binding to lectin, triggering a dissociation of dextran that is proportional to the increase in glucose. In addition to Concanavalin (Con) A-dextran, one needs a special semi-permeable membrane that allows selective diffusion of glucose across the membrane, but that prevents the transport of larger molecules, such as peptides or proteins, or other potentially interfering molecules, such as lactate or polysaccharide, contained in body fluids [65]. Generally, cellulose acetate (CA), cellulose ester and polyamide (PA) membranes are used in glucose sensing application based on the osmosis principle [22, 23, 65, 66]. The cellulose membranes present chemical and biological resistances to the body and are not suitable for a long-term implant. Anodic aluminum oxide (AAO) membranes have found acceptance for a wide range of bio-medical applications [23, 65].

5.4 Summary

The concept of osmosis based pressure sensor is extended to a specific application of glucose sensing. We have demonstrated a device to measure changes in glucose concentrations outside with respect to the reference solution of 100 mg/dL inside the cavity. A system in which piezoresistive pressure sensor was attached to a fluidic test chamber and a test setup was prepared to measure the glucose concentration levels in the test chamber. The performance of the fabricated device was studied for different glucose concentration levels. A sensitivity of 1 μV to 2 μV/(V·mg/dL·min) was obtained for device having membrane thickness of 10 μm compared to 0.3 μV to 0.5 μV/(V·mg/dL·min) for 25 μm thick membrane, without any amplification of the output voltage. The simulation and experimental results were closely matched. The response time of the designed devices was found to be smaller and the output voltage corresponding the glucose concentration variation was found to be proportional.

6

Design of Controlled Drug Delivery Pump for Insulin Delivery Application

Contents

6.1 Introduction

Insulin pumps are used to deliver exogenous insulin to compensate lack of indigenous insulin from the pancreas. These pumps act as artificial pancreas for delivering insulin but they cannot sense glucose levels automatically, like the pancreas in a human body. There are different ways to take the insulin into the human body, most popular methods are intravenous, subcutaneous, and intraperitoneal routes [4]. In all these external infusion techniques, infection risks are very high. The advancement in the field of micro-machining technology has led the design of miniature devices for the controlled insulin delivery. Many kinds of micro-pumps have been

proposed for the drug delivery applications, particularly where devices are used in the field of chemical and bioanalytical sciences [67]. Different types of techniques are developed to pump the fluids at microscale, which incorporates mechanical propulsion driven by the pressure or the piezoelectric phenomena, electro-wetting, thermo-capillary pumping, electro-hydrodynamic pumping, and an AC electro-osmosis. However, the disadvantage of those systems are the use of external energy; such as pressure, temperature gradients or high applied voltages; others use moving elements or produce pulsating flow.

The conventional insulin delivery pumps use mechanical strokes [17] to deliver insulin and it may leads to error in the infusion because of the aging problems in the mechanical parts. In this chapter, we present the design of an AC electro-osmotic pump for the insulin delivery application. The AC electro-osmotic micro-pumps seem to be promising for the drug delivery at micro and nano-scale, due to the absence of moving parts and it is relatively easy to integrate with a glucose sensor. The micro-pump employed in this work differs from others in the literature in the following ways. The flow velocity is increased by increasing the number of electrodes which are placed on both sides of the channel wall [68, 69]. The drug delivery rate will be constant if all the electrodes are arranged into a single set. In order to vary the drug delivery rate, the electrodes are arranged into four sets. This method produces different flow rates from a constant power source. A controlled drug delivery is achieved by switching the input voltage from set1 to set4 according to the insulin delivery requirements. Moreover, the electrodes in the micro-pump are driven by low amplitude AC voltage of low frequency f_0 and therefore suitable for low power portable devices. The low frequency is chosen to avoid the any transient effects and to maintain the unidirectional fluid flow. An additional advantage of employing low-voltage is the absence of electrolysis in the system. The sections of this chapter are as follows. The basics of electro-osmosis principle and the design details of electro-osmotic pump explained in section 6.2 and 6.3 respectively. Simulation results of an electro-osmotic pump is discussed in section 6.4 and finally the chapter is summarized in section.

6.2 Electro-osmosis Theory

Electro-kinetic phenomena are widely used for transfer of liquids at the micro/nanoscales and are essential components in microfluidic lab-on-a-chip devices because they contain no moving parts [69]. A periodic array of electrodes are designed onto an insulator substrate (glass) as show in Fig. 6.1. The electrodes are of equal width and are driven by a AC signal of four phase. When a fluid is introduced into a microchannel, the surface charge density induces the formation of a double layer in the fluid by attracting oppositely charged ions from the electrolyte to the immediate vicinity of the wall. The magnitude of this charged double layer is governed by the zeta potential of the channel liquid pair. When the chamber is filled with a liquid (electrolyte + insulin) having the conductivity σ and permittivity ϵ, part of its solid surface acquires a surface charge, known as an electric double layer which is formed at the fluid solid interface and its characteristic thickness is negligibly small ($\sim$ 10 nm) compared to the other dimensions of the micro-pump. When an AC voltage is applied to the electrodes, the electric field generates an induced charge in the double layer. The electric field acts on the charge, pulls the fluid in the direction of the traveling wave, giving rise to a net fluid flow [69].

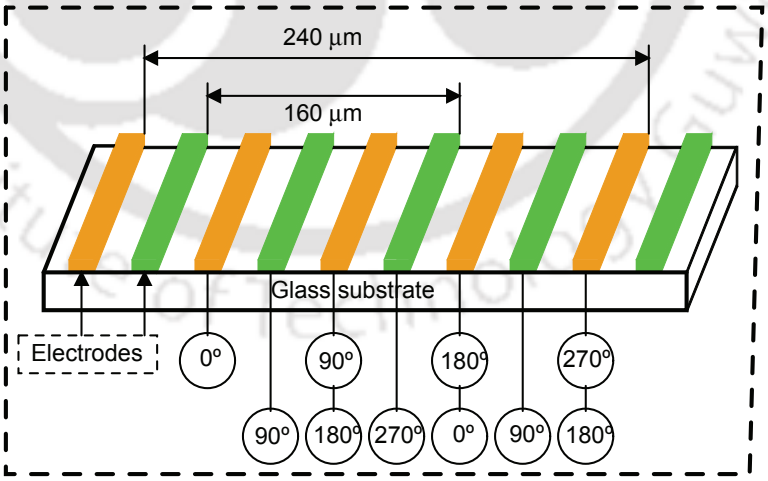

Figure 6.1: A periodic array of microelectrodes.

The AC low voltage is chosen such that the Faradaic currents from electrode to electrolyte are absent. Indeed, the power supply is a major concern for the biomedical devices because

the lifetime and size of the system is affected by battery durability. Therefore, operation under low voltages, improves the lifetime and size. The frequency of the applied signal is low enough, i.e. $\omega\lambda_D^2/D \ll 1$, the double layer in quasi-equilibrium. Here ω is the angular frequency, D is the mean diffusion coefficient of the ions and $\lambda_D^2 = \epsilon/\sigma$ is the time an ion takes to travel the Debye length by diffusion. The ions can equilibrate locally, for periods of the applied signal much greater than λ_D^2/D. The flow velocity of the micro-pump depends on the frequency and amplitude of the applied signal, and on the electrolyte conductivity. The fluid velocity will be zero both at low and high frequencies [70], because most of the applied voltage is dropped across the double layer and bulk electrolyte, respectively. The typical transition frequency, f_0, is much smaller than the charge relaxation frequency of the bulk electrolyte.

$$f_0 = \frac{\sigma}{2 \cdot \pi \cdot \epsilon} \tag{6.1}$$

where σ and ϵ are the electrical conductivity and permittivity of the electrolyte, respectively. The fluid velocity at the surface of the electrodes has been formulated by the Helmholtz-Smoluchowski. The relation between electro-osmotic velocity and the tangential component of the applied electric field is given by the equation.

$$v = \frac{\epsilon \cdot \Delta\phi}{\eta} E_x \tag{6.2}$$

where η is the viscosity of the fluid, $\Delta\phi$ is the potential drop across the diffuse double layer and E_x is the tangential electric field outside the double layer.

6.3 Design of an Electro-osmotic Pump

The insulin pump is an AC electro-osmotic pump with traveling wave electrode arrays as shown in Fig. 6.2. The micro-pump consists of an array of 48 interdigitated electrodes coated on a glass substrate. The electrodes are 20 μm wide and separated by distance of 20 μm. These electrodes are arranged into four sets as shown in Fig. 6.2. The electro-osmotic pump can be integrated with glucose sensor since there is no moving parts involved, and therefore the insulin delivery is easily auto-regulated with the help of a control unit, if the glucose concentration levels

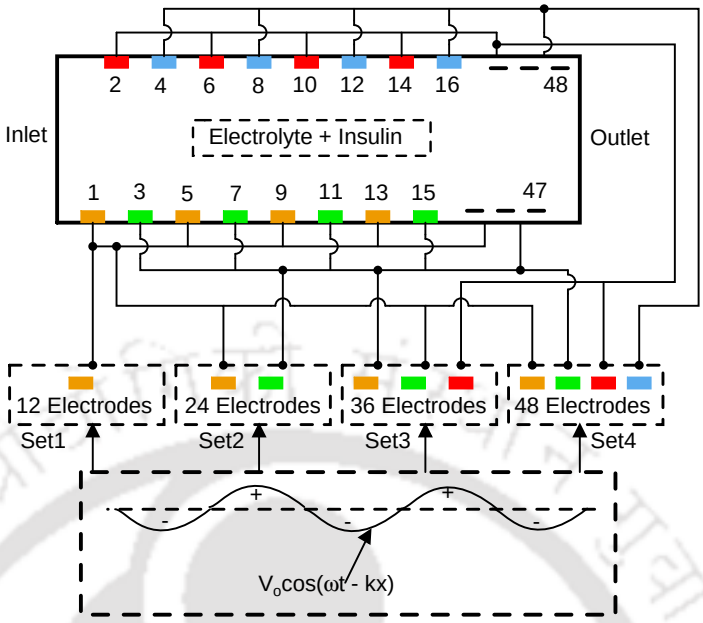

Figure 6.2: AC electro-osmotic pump for controlled drug delivery.

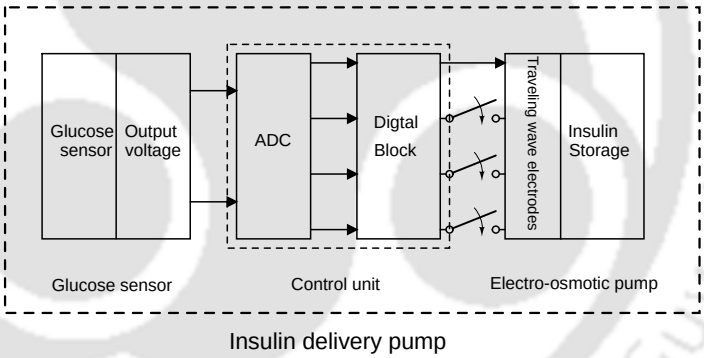

Figure 6.3: Insulin delivery system.

are ceaselessly monitored. Fig. 6.3 shows the glucose sensor is integrated with electro-osmotic pump through a control unit. Generally, the output voltage of the glucose sensor increases corresponding to the change glucose concentration levels in the human body from a normal level. The advantage of this method is that the micro-pump delivers the insulin with different flow rates according to the level of glucose concentration. The set1 operates continuously to provide the background minimum insulin needed for the patient. If the glucose concentration levels are increased after the food intake, the input voltage is switched from set1 to set2-set4

depending on the insulin requirements.

6.4 Simulation Results

The main aim of the simulations is to understand and optimize the each parameter of the electro-osmotic pump to achieve the desired results. The simulations are carried out using a commercially available MEMS software tools. Initially, the electro-osmotic pump 2D model is created and the meshing has been achieved using the triangular elements. The extremely fine mesh is employed where the fluid is interacting with the electrodes on the glass substrate, and the normalized mesh is used for the remaining part to improve the computational speed. The electro-osmotic pump is simulated with a electrolyte fluid, and corresponding fluid properties are assigned. The electrolyte fluid considered in this work is potassium chloride (KCl) with a conductivity of 1.3×10^{-3} S/m and a permittivity of $80.2\times\epsilon_0$. The Navier-Strokes equation describes the fluid flow in the micro-pump. The boundary conditions for the electro-osmotic pump are assigned. The pressure at the inlet is specified as zero. The fluid velocity at the outlet depends on the applied input voltage and frequency. The fluid velocity at the glass surface is zero. The applied input voltage is 1 V peak-to-peak at a frequency of 500 Hz. The input AC voltage on consecutive electrodes is phase-shifted by 90 degrees. This produces a traveling wave potential having a wavelength of 160 μm and 240 μm as shown in Fig. 6.1. Each electrode in the set is driven with an input AC voltage when it is operated and the electrodes in other sets are grounded. The set1 consists of 12 electrodes and these are 20 μm wide and separated by a distance of 40 μm.

Initially, the fluid flow velocity across the outlet of the micro-pump is 32 μm/s approximately, when the set1 is operated as shown in Fig. 6.4. The fluid velocity is increased from 32 to 107 μm/s as per the requirements by switching the input voltage from set1 to set4 as shown in Fig. 6.5. But the same is not possible with a single set of electrodes and it can deliver the insulin with a constant flow rate. The insulin delivery is auto-regulated by switching the voltage between the four sets according to the glucose concentration levels. The height of the electro-osmotic pump has the great influence on the fluid flow velocity at the outlet of

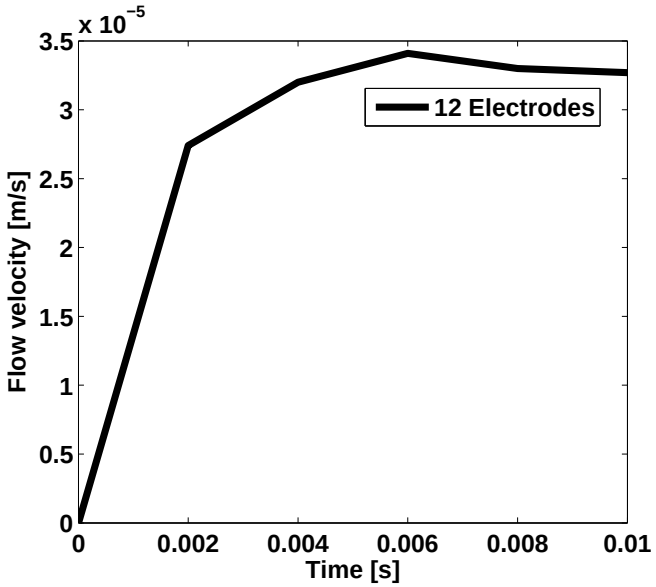

Figure 6.4: The fluid velocity at the outlet of the micro-pump when the set1 is operated.

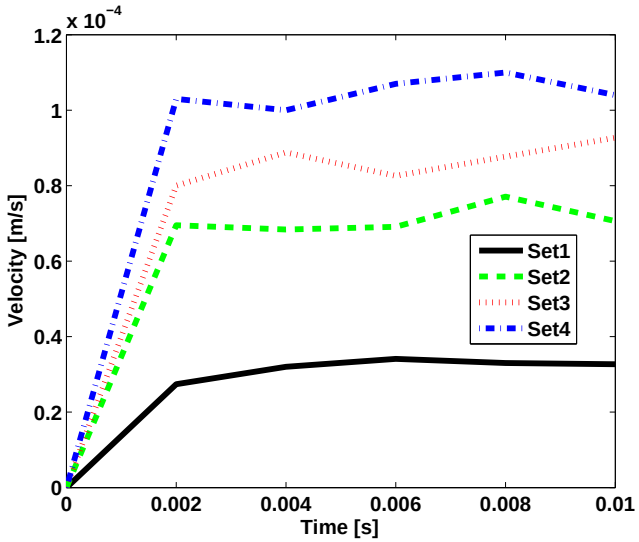

Figure 6.5: Flow velocity at the outlet of the micro-pump.

the micro-pump. Fig. 6.6 plots the horizontal fluid velocity as function of height above the electrodes. The pump behavior is analyzed in terms of voltage and frequency by measuring the fluid velocity with respect to the height above the electrodes.

In an AC electro-osmotic pump, the geometry of the device influences the overall pumping performance in more than one way. Unlike a DC electro-osmotic pump, where the velocity is

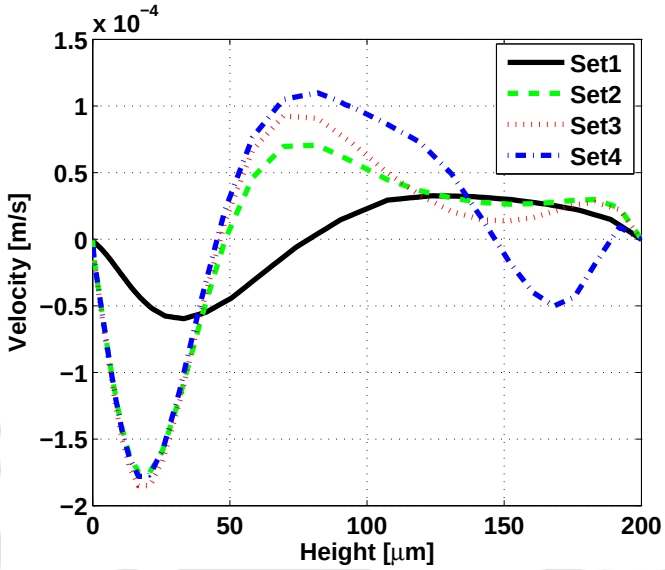

Figure 6.6: Flow velocity versus height of the micro-pump.

maximum and constant over the entire cross-section, AC electro-osmotic pump gives an oscillating flow velocity. The geometrical effect is that the outlet height can induce flow recirculation within the pumping channel, when the outlet height is smaller than the micro-pump [69]. If the outlet is smaller than the micro-pump, its hydraulic resistance will be larger and a portion of the liquid will circulate back in the upper part of the micro-pump, where it encounters a smaller resistance. In addition, the electrodes lie on the same plane, and the shape of the applied electric field is circular [71] and the motion of the liquid immediately above the surface of the electrode will follow such a shape. The fluid velocity is moving opposite direction when the height of micro-pump is above 140 μm. The height of the micro-pump and chamber width are optimized to 140 μm and 300 μm, respectively.

6.5 Summary

The AC electro-osmotic pump was designed to provide the controlled drug delivery. The micro-pump consists of a 48 electrodes and these were arranged into four sets to provide the different flow rates with a constant source. The flow velocity at the outlet of the electro-osmotic pump was increased from 32 to 107 μm/s, when the input voltage changed from set1 to set4.

The height and width of the micro-pump was 140 μm and 300 μm respectively. This electro-osmotic pump has the potential to deliver the insulin according to glucose concentration levels if it is integrated with a continuous glucose monitoring system.

7 Conclusion

Contents

7.1 Conclusion

The work carried out in this thesis was divided into two parts. The first part presented the design of a high sensitivity SiO_2 microbridge. The second part presented the main contribution of the thesis i.e. the design, fabrication, packaging and testing of a chemical-free osmotic pressure sensor to measure the change in glucose concentration levels.

An osmotic pressure sensor was designed to measure the change in glucose concentration levels. The structural and electrical behavior of device, and the fluid flow through the semi-permeable membrane were analyzed using commercially available FEM and FVM software tools. The relation between the fluid structure interaction was studied by coupling three different equations (Navier-Strokes equation, ALE, and theory of elasticity). The effect of geometrical parameters on the device performance were observed through the simulation studies.

By considering the response time, linearity and sensitivity, finally, two devices having different diaphragm thickness of 10 μm and 25 μm, but with the same area of 3 mm $\times$ 3 mm were chosen.

The designed osmotic pressure sensor was fabricated using bulk micro-machining technology. The device was packaged in a cavity made on PC material by employing a simple technique. The packaging cost was low because of the PC material and it does not need steps like a laser dicing, lithography, etching, or anodic bonding. The temperature employed to house the device in the cavity on PC material was low there by thermally induced stress is reduced.

The concept of osmosis based pressure sensor is extended to a specific application of glucose sensing. We have demonstrated a device to measure changes in glucose concentrations outside with respect to the reference solution of 100 mg/dL inside the cavity. A sensitivity of 1 μV to 2 μV/(V·mg/dL·min) was obtained for device having membrane thickness of 10 μm compared to 0.3 μV to 0.5 μV/(V·mg/dL·min) for 25 μm thick membrane, without any amplification of the output voltage. The simulation and experimental results were closely matched. The response time of the designed devices was found to be smaller and the output voltage corresponding the glucose concentration variation was found to be proportional. Finally, an AC electro-osmotic pump was designed which provide the controlled drug delivery. The micropump consists of a 48 electrodes and these were arranged into four sets to provide the different flow rates, but operated from a single power source. The flow velocity at the outlet of the electro-osmotic pump was increased from 32 to 107 μm/s, when the input voltage switched from set1 to set4.

7.2 Future Work

Continuous monitoring of glucose concentration levels and continuous insulin delivery are very challenging tasks. The design of a control unit and its integration with an electro-osmotic pump and a glucose sensor for continuous insulin delivery may be investigated. An auto-regulated insulin delivery, with different flow rates, according to glucose concentration levels can be the goal of such a system.

The present work can be extended to the design and fabrication of an artificial pancreas.

Two different devices may be fabricated on the same substrate, one is an osmotic pressure sensor and other is a micro-actuator. For the osmotic pressure sensor, one can employ glucose in solution form and for microactuator purpose, one can use a gel type smart material which has glucose affinity. The displacements occur in both devices are used for a controlled drug delivery if the microfluidic pump is attached to the movable membrane of the sensor. Thereby, the response time and selectivity may be improved.

Design of a surface acoustic wave (SAW) device may be investigated for glucose sensing application. The glucose affinity smart material can be employed as sensing material in this case also. The advantages of such a system will be its high selectivity, low response time and simple fabrication process.

7.3 List of Publications

International Journals

- Nagesh Ch and Roy Paily, "High Sensitivity Microbridge for Molecular Sensing Applications, International Conference on Design and manufacturing", IConDM 2013, Procedia Engineering, Elsevier, Volume 64, Pages 234-243, 2013.
- Nagesh Ch and Roy Paily, "Fabrication and Testing of an Osmotic Pressure Sensor for Glucose Sensing Application." Micromachines 5, No. 3: 722-737, 2014.
- Nagesh Ch and Roy Paily, "Design of an Osmotic Pressure Sensor for Sensing Osmotically Active Substance". J. Micromech. Microeng, Volume 25, No 04, 5019 (PP9), 2015.

National/International Conferences

- Nagesh Ch and Roy Paily, "FEM AND FVM Simulations of Osmotic Microactuator", fifth ISSS National Conference on MEMS, Smart Materials Structures and Systems, Karpagam University, Coimbatore, India, September, 2012.
- Nagesh Ch and Roy Paily, "A Cost-effective Piezoresistive Pressure Sensor Packaging

for Biomedical Applications", Seventh ISSS International Conference on Smart Materials Structures and Systems, Indian Institute of Science, Bangalore, India, 2014.

- Nagesh Ch and Roy Paily, "Design of an Electro-osmotic Pump for Controlled Drug Delivery", International Conference on MEMS and Sensors, IIT Madras, Chennai, India, 2014.

Bibliography

[1] T. Koschinsky, L. Heinemann, "Sensors for glucose monitoring: technical and clinical aspects," *Diabetes/Metabolism Research and Reviews*, vol. 17, no. 2, pp. 113–123, 2001.

[2] J. C. Pickup, F. Hussain, N. D. Evans, O. J. Rolinski, and D. J. Birch, "Fluorescence-based glucose sensors," *Biosensors and Bioelectronics*, vol. 20, no. 12, pp. 2555 – 2565, 2005, 20th Anniversary of Biosensors and Bioelectronics 20th Anniversary of Biosensors and Bioelectronics.

[3] J. Wang, "Electrochemical glucose biosensors," *Chemical Reviews*, vol. 108, no. 2, pp. 814–825, 2008, pMID: 18154363.

[4] D. Takahashi, Y. Xiao, F. Hu, M. Lewis, "A survey of insulin-dependent diabetes-part i: Therapies and devices," *Int. J. Telemedicine Appl.*, vol. 2008, pp. 1–15, 2007.

[5] S. Updike, G. Hicks, "The enzyme electrode," *Nature*, vol. 214, pp. 986–988, 1967.

[6] "Ysi 2300 stat plus^{TM} glucose & lactate analyzer," *Y S I Life Sciences, Inc., Ohio, USA*. [Online]. Available: http://www.ysilifesciences.com/index.php?page=ysi-2300-stat-plus-glucose-lactate-analyzer

[7] "Minimed paradigm real-time® revel system," *Medtronic MiniMed, Inc., San Antonio, TX, USA*. [Online]. Available: http://www.minimed.com/products/insulinpumps/index.html

[8] "Freestyle insulinx blood glucose monitoring system," *Abbott Diabetes Care, Inc., Alameda, CA, USA*. [Online]. Available: http://www.abbottdiabetescare.com

[9] "Dexcom g4 platinum," *Dexcom, Inc., San Diego, CA, USA*, 2009. [Online]. Available: http://www.dexcom.com/

[10] X. Huang, S. Li, J. S. Schultz, Q. Wang, and Q. Lin, "A mems affinity glucose sensor using a biocompatible glucose-responsive polymer," *Sensors and Actuators B: Chemical*, vol. 140, no. 2, pp. 603 – 609, 2009.

[11] X. Huang, S. Li, J. Schultz, Q. Wang, and Q. Lin, "A capacitive mems viscometric sensor for affinity detection of glucose," *Microelectromechanical Systems, Journal of*, vol. 18, no. 6, pp. 1246–1254, Dec 2009.

[12] J. Pei, F. Tian, and T. Thundat, "Glucose biosensor based on the microcantilever," *Analytical Chemistry*, vol. 76, no. 2, pp. 292–297, 2004, pMID: 14719873.

[13] F. T. Jianhong Pei and T. Thundat, "Novel glucose biosensor based on the microcantilever," *Materials Research Society*, vol. 776, pp. Q11.21.1–Q11.21.5, 2003.

[14] A. Subramanian, P. I. Oden, S. Kennel, K. B. Jacobson, R. Warmack, T. Thundat, and M. Doktycz, "Glucose biosensing using an enzyme-coated microcantilever," *Applied Physics Letters*, vol. 81, pp. 385–387, 2002.

[15] S. Vogel, *Cats' Paws and Catapults*. W. W. Norton & Company, Inc., 1998.

[16] F. Naftel, "Implantable device for estimating glucose levels," U S Patent 5 337 747, 1994.

[17] T. Nagakura, K. Ishihara, T. Furukawa, K. Masuda, and T. Tsuda, "Auto-regulated osmotic pump for insulin therapy by sensing glucose concentration without energy supply," *Sensors and Actuators B: Chemical*, vol. 34, pp. 229 – 233, 1996.

[18] O. Ellingsen, "Method for monitoring the level of an osmotically active component in body fluid and device for carrying out said method," U S Patent 6 224 550 B1', 2001.

[19] Y.-C. Su, L. Lin, and A. Pisano, "A water-powered osmotic microactuator," *Microelectromechanical Systems, Journal of*, vol. 11, no. 6, pp. 736–742, Dec 2002.

[20] Y.-C. Su and L. Lin, "A water-powered micro drug delivery system," *Microelectromechanical Systems, Journal of*, vol. 13, no. 1, pp. 75–82, Feb 2004.

[21] G. Lin, S. Chang, H. Hao, P. Tathireddy, M. Orthner, J. Magda, and F. Solzbacher, "Osmotic swelling pressure response of smart hydrogels suitable for chronically implantable glucose sensors," *Sensors and Actuators B: Chemical*, vol. 144, no. 1, pp. 332 – 336, 2010.

[22] O Krushinitskaya, T I TØnnessen, H Jakobsen and Erik Johannessen, "The assessment of potentially interfering metabolites and dietary components in blood using an osmotic glucose sensor based on the concanavalin a-dextran affinity assay," *Biosensors and Bioelectronics*, vol. 28, no. 1, pp. 195 – 203, 2011.

[23] E Johannessen, O Krushinitskaya, A Sokolov, P Hfliger, A Hoogerwerf, C Hinderling, K Kautio, J Lenkkeri, E Strmmer, V Kondratyev, T I Tnnessen, T E Mollnes, H Jakobsen, E Zimmer, and B Akselsen, "Toward an injectable continuous osmotic glucose sensor," *Journal of Diabetes Science and Technology*, vol. 4, pp. 882–892, 2010.

[24] Y. Lu, V. Chivukula, M. Wang, and H.-F. Ji, "Simulation and fabrication of SiO_2-based piezoresistive microbridges for chem/biosensors," *Journal of Micromechanics and Microengineering*, vol. 16, no. 4, p. 692, 2006.

[25] F. Theeuwes and S. Yum, "Principles of the design and operation of generic osmotic pumps for the delivery of semisolid or liquid drug formulations," *Annals of Biomedical Engineering*, vol. 4, no. 4, pp. 343–353, 1976.

[26] V. T.-C. Michel Godin and P. Grutter, "Quantitative surface stress measurements using a microcantilever," *Applied Physics Le*, vol. 79, no. 4, pp. 551–553, July 2001.

[27] D. W. D. T. Thundat, "Simulation of adsorption-induced stress of a microcantilever sensor," *Journal of Applied Physics*, vol. 97, p. 043526, 2005.

[28] F. T. Jianhong Pei and T. Thundat, "Glucose biosensor based on the microcantilever," *Analytical Chemistry*, vol. 76, no. 2, pp. 292–297, 2004.

[29] S. J. K. K. B. J. R. J. W. T. T. A. Subramanian, P. I. Oden and M. J. Doktycz, "Glucose biosensing using an enzyme-coated microcantilever," *Applied Physics Letters*, vol. 81, pp. 385–387, May 2002.

[30] G. M. B. Xiaohe Xu, Thomas G. Thundat and H.-F. Ji, "Detection of Hg^{2+} using microcantilever sensors," *Anal. Chem.*, vol. 74, pp. 3611–3615, 2002.

[31] C. M. O. N. Gabriel Vasile, Cristian Lepadatu, "Simulation and design of a resonant polysilicon microbridge," pp. 573–576, 2001.

[32] Y. Tang, J. Fang, X. Yan, and H.-F. Ji, "Fabrication and characterization of SiO_2 microcantilever for microsensor application," *Sensors and Actuators B: Chemical*, vol. 97, no. 1, pp. 109–113, 2004.

[33] D. D. Bogdan Firtat, Carmen Moldovan, "Microbridges simulation for piezoresistive gas sensors detection," pp. 63–66, 2002.

[34] Y. Tang, J. Fang, X. Xu, H.-F. Ji, G. M. Brown, and T. Thundat, "Detection of femtomolar concentrations of hf using an SiO_2 microcantilever," *Analytical Chemistry*, vol. 76, no. 9, pp. 2478–2481, 2004, pMID: 15117186. [Online]. Available: http://pubs.acs.org/doi/abs/10.1021/ac035140g

[35] Q. R. Yin Zhang and Y. pu Zhao, "Modelling analysis of surface stress on a rectangular cantilever beam," *Journal of Physics D: Applied Physics*, vol. Phys. 37, pp. 2140–2145, 2004.

[36] J. M. Gere, *Mechanics of Materials*. CENGAGE Learning, 2006.

[37] C. Inc., "Supplemental tutorials and reference guide," pp. R8 1 – R8 6, 2010.

[38] S. Yang and C. Chang, "A piezoresistive bridge-microcantilever biosensor by {CMOS} process for surface stress measurement," *Sensors and Actuators B: Chemical*, vol. 145, no. 1, pp. 405 – 410, 2010.

[39] X. Zhao, "Modeling and simulation of mems devices," Ph.D. dissertation, Virginia Polytechnic Institute and State University, 2004.

[40] M. Tabib-Azar, "Optically controlled silicon microactuators," *Nanotechnology*, vol. 1, pp. 81–92, 1990.

[41] D. Dissanayake, S. Al-Sarawi, and D. Abbott, "Electrostatic microactuator design using surface acoustic wave devices," in *Smart Sensors and Sensing Technology*, ser. Lecture Notes Electrical Engineering, S. Mukhopadhyay and G. Gupta, Eds. Springer Berlin Heidelberg, 2008, vol. 20, pp. 139–151. [Online]. Available: http://dx.doi.org/10.1007/978-3-540-79590-2_10

[42] A. Nisar, N. Afzulpurkar, B. Mahaisavariya, and A. Tuantranont, "Mems-based micropumps in drug delivery and biomedical applications," *Sensors and Actuators B: Chemical*, vol. 130, no. 2, pp. 917 – 942, 2008. [Online]. Available: http://www.sciencedirect.com/science/article/pii/S0925400507009148

[43] G. A. A. Rodrguez, C. Rossi, and K. Zhang, "Multi-physics system modeling of a pneumatic micro actuator," *Sensors and Actuators A: Physical*, vol. 141, no. 2, pp. 489 – 498, 2008. [Online]. Available: http://www.sciencedirect.com/science/article/pii/S0924424707005894

[44] C. Tsou, "The design and simulation of a novel out-of-plane micro electrostatic actuator," *Microsystem Technologies*, vol. 12, no. 8, pp. 723–729, 2006. [Online]. Available: http://dx.doi.org/10.1007/s00542-006-0107-1

[45] T. Y. Cath, A. E. Childress, and M. Elimelech, "Forward osmosis: Principles, applications, and recent developments," *Journal of Membrane Science*, vol. 281, pp. 70 – 87, 2006.

[46] P. W. Atkins, *Physical Chemistry*, 5th ed. Oxford: Oxford University Press, 1994.

[47] D. A. Nield and A. Bejan, *Convection in Porous Media*, thrd edition ed. Sprin, 2006.

[48] R. P. Durbin, "Osmotic flow of water across permeable cellulose membranes," *J. Gen. Physiol.*, vol. 44, pp. 315–326, 1960.

[49] M. Narayanaswamy, R. J. Daniel, K. Sumangala, and C. A. Jeyasehar, "Computer aided modelling and diaphragm design approach for high sensitivity silicon-on-insulator pressure sensors," *Measurement*, vol. 44, no. 10, pp. 1924 – 1936, 2011.

[50] E. Bakhoum and M. Cheng, "Novel capacitive pressure sensor," *Microelectromechanical Systems, Journal of*, vol. 19, no. 3, pp. 443–450, June 2010.

[51] K. N. Bhat, "Silicon micromachined pressure sensors," *J. IISc.*, vol. 87, pp. 115–131, 2007.

[52] S. D. Senturia, *Microsystem Design*. Kluwer Academic publishers, 2001.

[53] J. S. Lee, F. Faheem, J. T. Kim, J. D. Jung, J. Y. Kim, J. D. Kim, and C. H. Lee, "A cost-effective mems cavity packaging technology for mass production," *Advanced Packaging, IEEE Transactions on*, vol. 32, no. 2, pp. 453–460, 2009.

[54] S. Walwadkar and J. Cho, "Evaluation of die stress in mems packaging: Experimental and theoretical approaches," *Components and Packaging Technologies, IEEE Transactions on*, vol. 29, no. 4, pp. 735–742, 2006.

[55] C. O'Neal, A. Malshe, S. Singh, W. Brown, and W. Eaton, "Challenges in the packaging of mems," in *Advanced Packaging Materials: Processes, Properties and Interfaces, 1999. Proceedings. International Symposium on*, 1999, pp. 41–47.

[56] J.-W. Joo and S.-H. Choa, "Deformation behavior of mems gyroscope sensor package subjected to temperature change," *Components and Packaging Technologies, IEEE Transactions on*, vol. 30, no. 2, pp. 346–354, 2007.

[57] Y.-M. Chiang, M. Bachman, and G. P. Li, "A wafer-level microcap array to enable high-yield microsystem packaging," *Advanced Packaging, IEEE Transactions on*, vol. 27, no. 3, pp. 490–496, 2004.

[58] X. Lou, Z. Li, and Y. Jin, "Plastic-silicon bonding for mems packaging application," in *Electronic Packaging Technology, 2006. ICEPT '06. 7th International Conference on*, 2006, pp. 1–3.

[59] C. Iliescu, H. Taylor, M. Avram, J. Miao, and S. Franssila, "A practical guide for the fabrication of microfluidic devices using glass and silicon," *Biomicrofluidics*, vol. 6, no. 1, pp. –, 2012. [Online]. Available: http://scitation.aip.org/content/aip/journal/bmf/6/1/10.1063/1.3689939

[60] B. Ziaie, A. Baldi, M. Lei, Y. Gu, and R. A. Siegel, "Hard and soft micromachining for biomems: review of techniques and examples of applications in microfluidics and drug delivery," *Advanced Drug Delivery Reviews*, vol. 56, no. 2, pp. 145 – 172, 2004, ¡ce:title¿Biosensing and Drug Delivery at the Microscale¡/ce:title¿. [Online]. Available: http://www.sciencedirect.com/science/article/pii/S0169409X03001911

[61] T. Velten, H. Ruf, D. Barrow, N. Aspragathos, P. Lazarou, E. Jung, C. Malek, M. Richter, J. Kruckow, and M. Wackerle, "Packaging of bio-mems: strategies, technologies, and applications," *Advanced Packaging, IEEE Transactions on*, vol. 28, no. 4, pp. 533–546, 2005.

[62] R. Narayan, Ed., *Biomedical Materials*. Springer, 2009.

[63] Y. Zhao, S. Li, A. Davidson, B. Yang, Q. Wang, Q. Lin, "A mems viscometric sensor for continuous glucose monitoring," *J. Micromech. Microeng.*, vol. 17, pp. 2528–2537, 2007.

[64] O. Ellingsen, B. E. Kulseng, Trondheim, H. Kristiansen, "Sensor in vivo measurement of osmotic changes," USA Patent US7 276 028 B2, 2007.

[65] H.A. Klok, and L. Lavanant, "Selectively permeable coated membrane," U S Patent 20 090 112 075 A1, 2009.

[66] O Krushinitskaya, T I T∅nnessen, H Jakobsen and Erik Johannessen, "Characterization of nanoporous membranes for implementation in an osmotic glucose sensor based on the concanavalin a-dextran affinity assay," *Journal of Membrane Science*, vol. 376, pp. 153 – 161, 2011.

[67] A. Ramos, A. Gonzlez, A. Castellanos, N.G. Green, and H. Morgan, "Pumping of liquids with ac voltages applied to asymmetric pairs of microelectrodes," *Phys Rev E*, vol. 67, p. 056302, 2003.

[68] J. Hrdlicka , P. Cervenka , M. Pribyl and D. Snita, "Zig-zag arrangement of four electrodes for ac electro-osmotic micropumps," *Phys Rev E*, vol. 84, p. 16307, 2011.

[69] P. Garcia-Sanchez, A. Ramos, N. G. Green, and H. Morgan, "Experiments on ac electrokinetic pumping of liquids using arrays of microelectrodes," *Dielectrics and Electrical Insulation, IEEE Transactions on*, vol. 13, no. 3, pp. 670–677, June 2006.

[70] A. Ramos, H. Morgan, N. G. Green, and A. Castellanos, "Ac electric-field-induced fluid flow in microelectrodes," *Journal of Colloid and Interface Science*, vol. 217, no. 2, pp. 420 – 422, 1999.

[71] N. G. G. A. Ramos, H. Morgan and A. Castellanos, "Ac electrokinetics: a review of forces in microelectrode structures," *Journal of Physics D - Applied Physics*, vol. 31, no. 18, p. 23382353, 1998.